CHAPTER 5

EFFECT OF ULTRASONIC SHOT PEENING ON HOT CORROSION BEHAVIOR OF Ti–6Al–4V ALLOY

5.1 INTRODUCTION

Degradation of materials from high-temperature oxidation and hot corrosion is the main cause of failure of the components in the hot sections of gas turbine engines [Subhash et al. (2015), Maya et al. (2014)]. Titanium alloys have been developed for high temperature applications with superior mechanical strength, corrosion resistance and fatigue resistance at elevated temperature. Alloy Ti–6Al–4V is commercially used for aerospace engine components working at about 400 °C. However, above 400 °C it oxidizes rapidly in oxygen containing environments and also undergoes hot corrosion in marine environment. Low grade fuel oils cause hot corrosion, forming Na_2SO_4 and V_2O_5 during combustion. Na_2SO_4 is produced from the reaction of NaCl in air and sulphur (present as impurity) in the fuel oil. Vanadium in the fuel oil in the form of vanadium porphyrin transforms into V_2O_5 during combustion [Mahobia et al. (2013)]. V_2O_5 and Na_2SO_4 form low temperature melting inorganic compounds which undergo eutectic reaction below 600 °C [Subhash et al. (2015)].

In this chapter, the effect of USSP on hot corrosion of the alloy Ti–6Al–4V under three different salt/mixed salts: 100wt.%NaCl, 75wt.%Na_2SO_4+25wt.%NaCl and 90wt.% Na_2SO_4+5wt.%NaCl+5wt.%V_2O_5 at 400, 500 and 600 ºC under cyclic heating

and cooling for 100h is discussed. The samples were subjected to 5 minute USSP for hot corrosion study.

Weight gain measurements were made to determine corrosion kinetics. Among the three types of salt/mixed salts 100%NaCl was found to be the most detrimental at 500 and 600 ºC. However, only minor weight change was observed at 400 ºC in the sample with 100%NaCl and there was negligible effect from the other two mixed salts. Corrosion rate was found to be less in the USSPed condition than that in the non-USSPed one. The degradation of corrosion resistance of the alloy Ti–6Al–4V occurred from the chemical reactions between titania and chloride ions, sulphur and vanadium present in the environments.

5.2 VISUAL OBSERVATIONS

Digital photographs of the test samples were recorded prior to exposure and after completion of the exposure cycles at 400, 500 and 600 ºC for 100h. Figure 5.1 shows the non-sprayed and salt/mixed salts sprayed samples, prior to exposure at elevated temperatures. Figures 5.2, 5.3 and 5.4 show corroded surfaces of the samples exposed at 400, 500 and 600 °C respectively. The color of surface of the non-USSPed and USSPed samples changed with the temperature of exposure. The non-USSPed/non-sprayed (bare) samples exposed at 400 and 500 °C were found to turn yellow/blue. However, the surfaces of the USSPed/non-sprayed samples exposed to 400 and 500 °C were observed to turn blue and grey respectively. The bright surface of the non-USSPed/non-sprayed sample turned brownish following the exposure at 600 °C whereas that of the USSPed sample exposed at 600 °C turned greyish.

Fig. 5.1 Digital photographs of the non-sprayed and salt/mixed salts sprayed samples prior to exposure at elevated temperatures.

The color of the both non-USSPed and USSPed samples sprayed with Type–1 salt and exposed at 400 °C was found whitish, however, from exposure at 500 and 600 °C was found whitish/blackish/brownish and also cracking was observed on the surface after 100h of exposure. Similar cracking was observed on the non-USSPed and USSPed samples, sprayed with Type–2 mixed salts and exposed at 600 °C and the color was blackish/whitish (Fig 5.4). Surface cracking was not observed on the Type–2 mixed salts sprayed non-USSPed and USSPed samples, exposed at 400 and 500 °C. The non-USSPed and USSPed samples sprayed with Type–3 mixed salts and exposed at 500 and 600 °C showed surface cracking and the color was turned greyish/brownish.

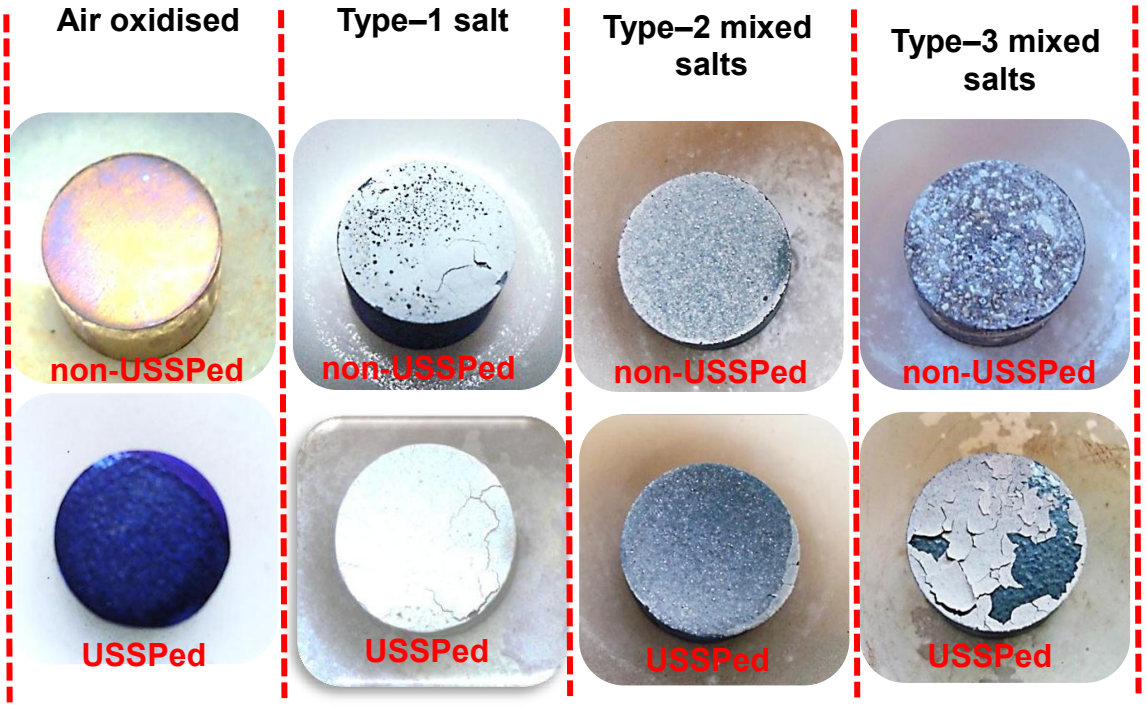

Fig. 5.2 Digital photographs of the non-USSPed and USSPed samples exposed at 400 °C for 100h.

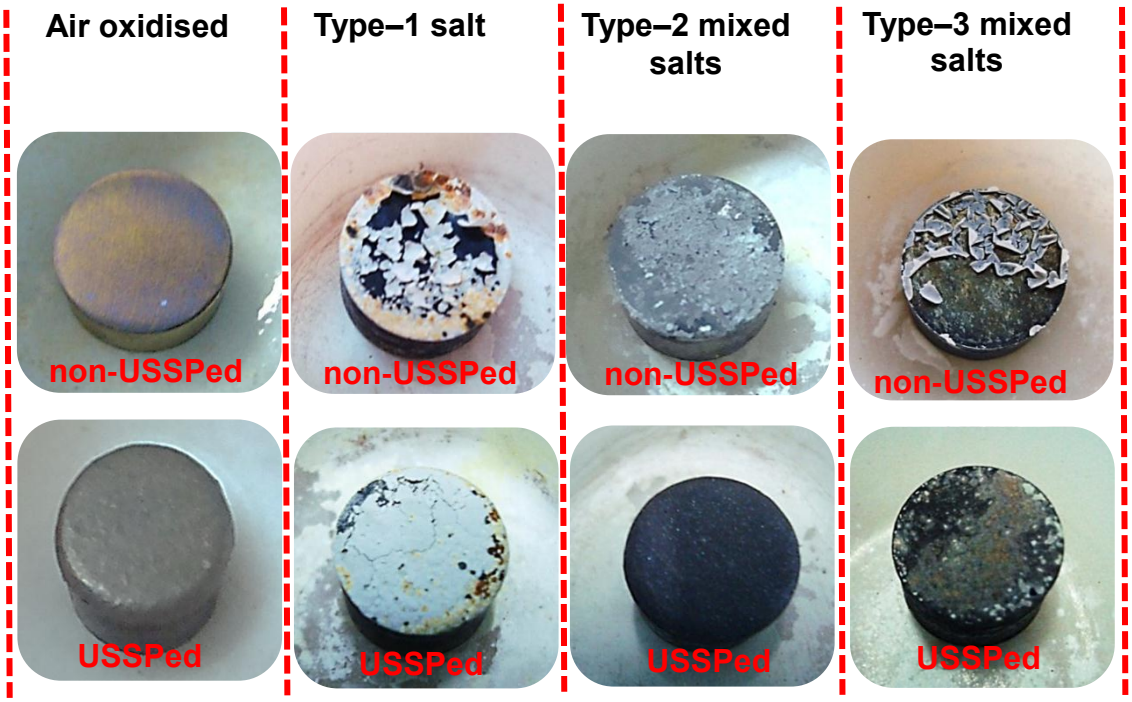

Fig. 5.3 Digital photographs of the non-USSPed and USSPed samples exposed at 500 °C for 100h.

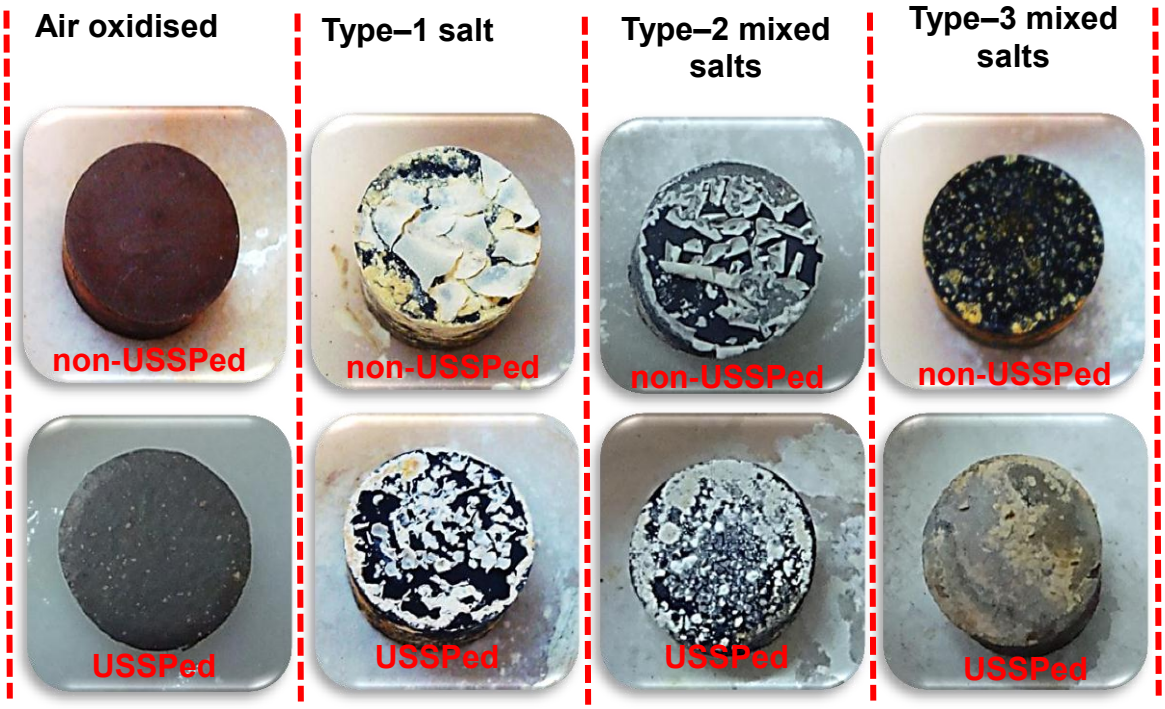

Fig. 5.4 Digital photographs of the non-USSPed and USSPed samples exposed at 600 °C for 100h.

5.3 CORROSION KINETICS

Weight gain plots show the effect of different salt/salt mixtures on hot corrosion behavior. There was very small change in weight of the Type–1 salt sprayed samples exposed at 400 ºC in the both non-USSPed as well as USSPed condition. On the other hand, weight gain was found to be negligible in the Type–2 and Type–3 mixed salts sprayed samples exposed at 400 ºC in the both non-USSPed as well as USSPed condition. However, significant weight gain was there in the both non-USSPed and USSPed samples exposed at 600 °C in comparison of the samples exposed at 500 °C. Samples sprayed with Type–1 salt showed highest weight gain, followed by those sprayed with Type–2 and Type–3 mixed salts, in the both non-USSPed as well as USSPed condition, exposed at 500 and 600 °C.

Figures 5.5-5.7 show variations of weight gain per unit area and square of weight gain per unit area with time of exposure, for the non-USSPed and USSPed samples exposed at 400 °C for a period of 100h. There was insignificant weight gain in the USSPed specimen from exposure at 400 °C.

The plots of square of weight gain/unit area (mg/cm^2) versus time (h) were used to establish rate law for the process of hot corrosion. The rate constant (k_p) was calculated from parabolic rate law equation [Raymond et al. (1992)]:

$$(\Delta W/A)^2 = k_p t + C \quad \text{..... (5.1)}$$

where $\Delta W/A$ is the weight gain per unit surface area (mg/cm^2), t is the time of exposure, and C is a constant. The curves of weight gain plots were best fitted by linear least-square method and the calculated values of k_P are presented in Table 5.1.

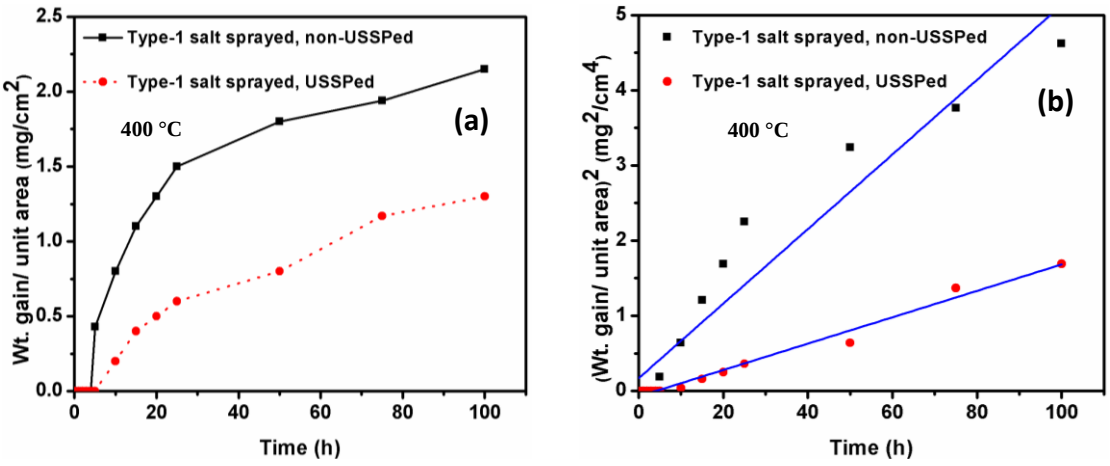

Fig. 5.5 Weight gain plots of Type–1 salt sprayed samples for the non-USSPed and USSPed conditions, exposed at 400 °C up to 100h: (a) weight gain per unit area vs time of exposure, (b) square of weight gain per unit area vs time of exposure.

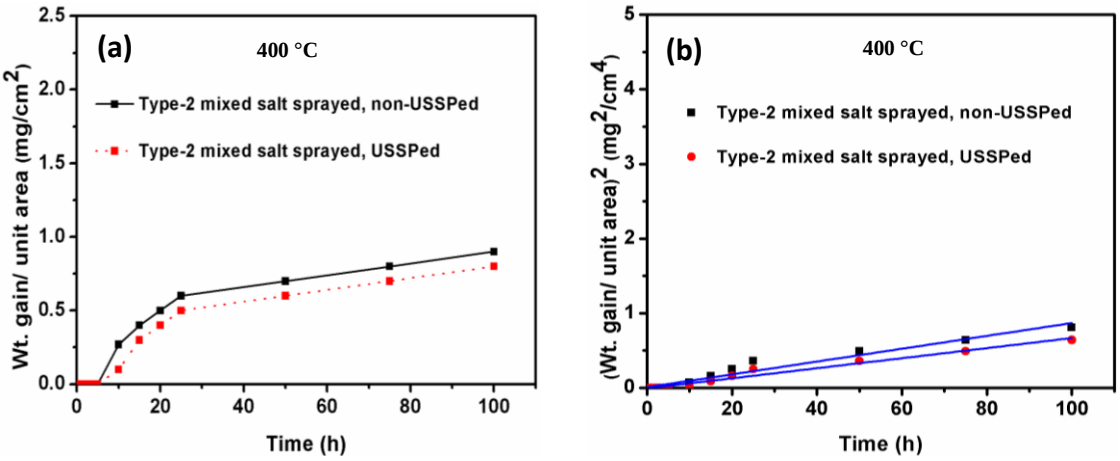

Fig. 5.6 Weight gain plots of Type–2 mixed salts sprayed samples for non-USSPed and USSPed conditions, exposed at 400 °C up to 100h: (a) weight gain per unit area vs time of exposure, (b) square of weight gain per unit area vs time of exposure.

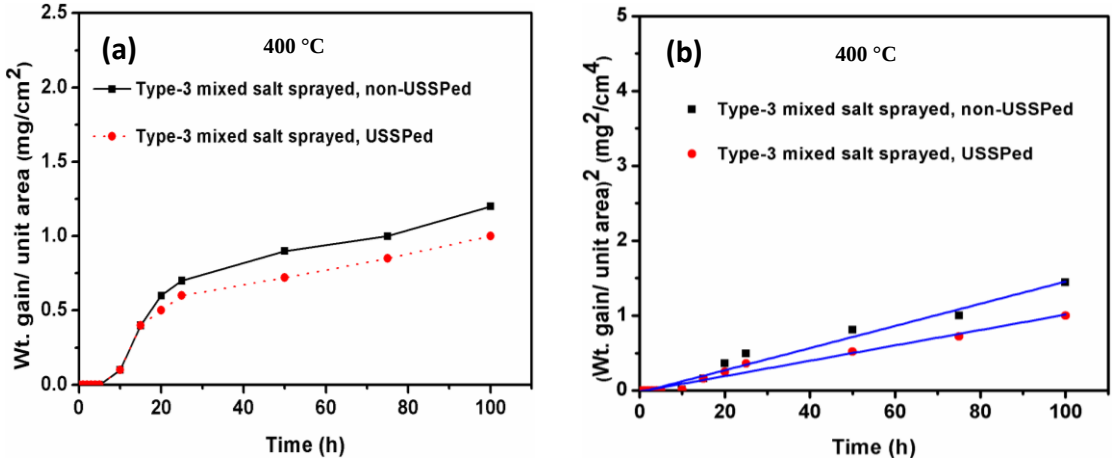

Fig. 5.7 Weight gain plots of Type–3 mixed salts sprayed samples for non-USSPed and USSPed conditions, exposed at 400 °C up to 100h: (a) weight gain per unit area vs time of exposure, (b) square of weight gain per unit area vs time of exposure.

Table 5.1 Parabolic rate constant (k_p) of the samples hot corroded at 400 °C for 100h.

Material condition	Type–1 salt Sprayed		Type–2 mixed salts sprayed		Type–3 mixed salts sprayed	
	$k_p(mg^2cm^{-4}h^{-1})$	R^2	$k_p(mg^2cm^{-4}h^{-1})$	R^2	$k_p(mg^2cm^{-4}h^{-1})$	R^2
non-USSPed	1.1215	0.92	1.019	0.95	1.0342	0.97
USSPed	1.0410	0.98	1.015	0.97	1.0231	0.97

There was little oxide layer on non-sprayed samples of the both non-USSPed and USSPed samples, exposed at 500 °C. Figures 5.8a, 5.9a and 5.10a show variation of weight per unit area with the duration of time for Type–1 salt, Type–2 mixed salts and Type–3 mixed salts sprayed exposed at 500 °C.

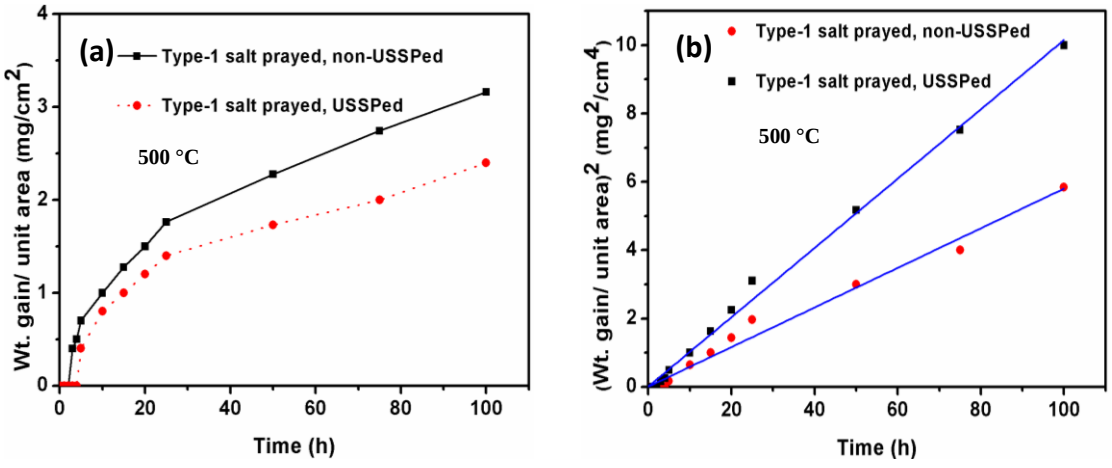

Fig. 5.8 Weight gain plots of Type–1 salt sprayed samples for non-USSPed and USSPed conditions, exposed at 500 °C up to 100h: (a) weight gain per unit area vs time of exposure, (b) square of weight gain per unit area vs time of exposure.

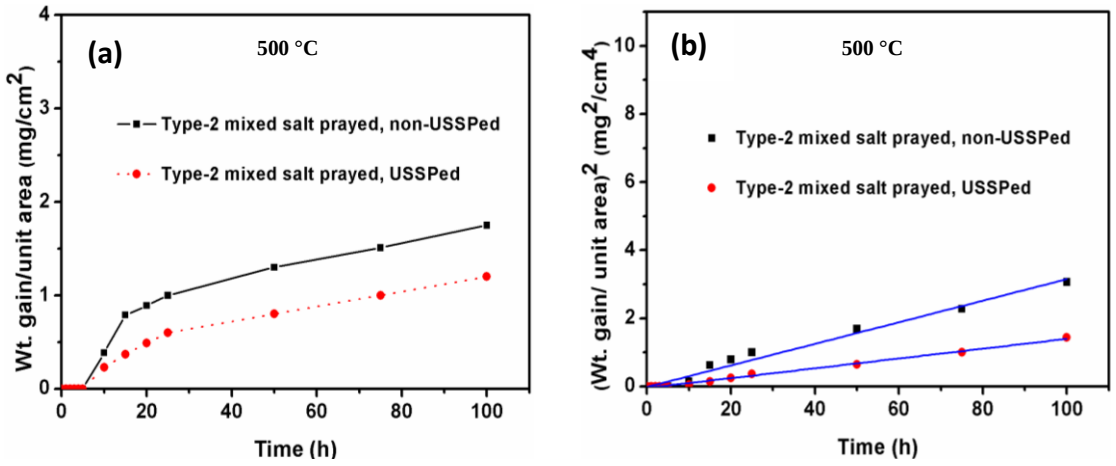

Fig. 5.9 Weight gain plots of Type–2 mixed salts sprayed samples for non-USSPed and USSPed conditions, exposed at 500 °C up to 100h: (a) weight gain per unit area vs time of exposure, (b) square of weight gain per unit area vs time of exposure.

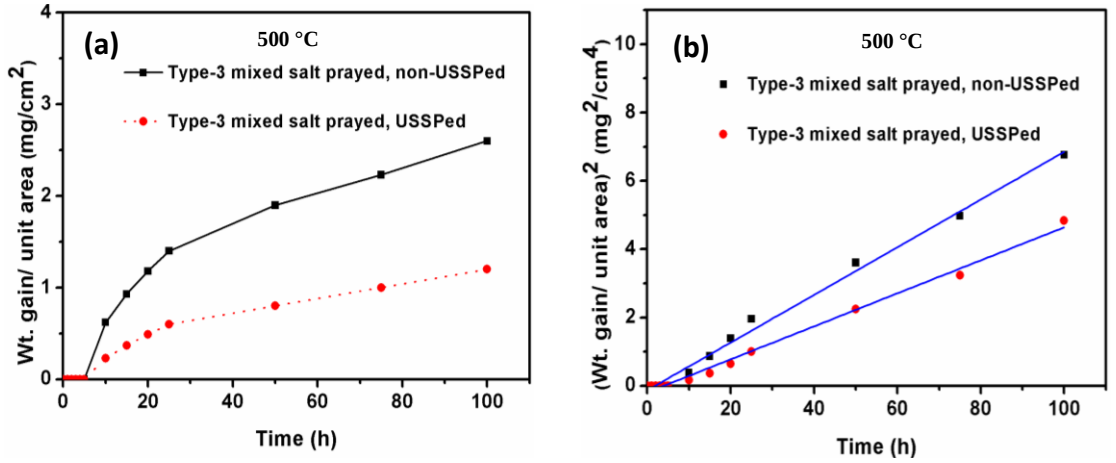

Fig. 5.10 Weight gain plots of Type–3 mixed salts sprayed samples for non-USSPed and USSPed conditions, exposed at 500 °C up to 100h: (a) weight gain per unit area vs time of exposure, (b) square of weight gain per unit area vs time of exposure.

The plots of weight-gain per unit area squared for the non-USSPed and USSPed samples sprayed with Type–1 salt, Type–2 mixed salts and Type–3 mixed salts, exposed at 500 °C with the time of exposure up to a period of 100h are shown in Figs. 5.8b, 5.9b and 5.10b respectively. The samples sprayed with Type–1 salt showed

highest weight gain, followed by those sprayed with Type–3 mixed salts and Type–2 mixed salts respectively, in the both non-USSPed as well as USSPed condition.

Type–1 salt sprayed samples and those sprayed with mixed salts of Type–2 and Type–3 showed linear variation in weight gain for the entire period of exposure. Table 5.2 shows calculated values of the parabolic rate constant (k_p) for the specimens sprayed with different salt/mixed salts and exposed at 500 °C.

Table 5.2 Parabolic rate constant (k_p) of the samples hot corroded at 500 °C for 100h.

Material condition	**Type–1 salt Sprayed**		**Type–2 mixed salts sprayed**		**Type–3 mixed salts sprayed**	
	$k_p(mg^2cm^{-4}h^{-1})$	R^2	$k_p(mg^2cm^{-4}h^{-1})$	R^2	$k_p(mg^2cm^{-4}h^{-1})$	R^2
non-USSPed	1.2639	0.99	1.0761	0.98	1.1709	0.99
USSPed	1.1260	0.96	1.0337	0.99	1.1241	0.99

Figure 5.11 shows oxidation behavior of the non-sprayed samples for non-USSPed and USSPed condition, exposed at 600 °C. It may be seen that the weight gain of non-sprayed sample was lower for the USSPed sample, exposed at 600 °C. It shows that corrosion resistance was improved from USSP. Figures 5.12-5.14 show variations of weight gain per unit area and square of weight gain per unit area with the duration of exposure for Type–1 salt, Type–2 and Type–3 mixed salts sprayed samples, exposed at 600 °C. Type–1 salt sprayed samples showed highest weight-gain followed by Type–3 and Type–2 mixed salts sprayed samples respectively, in the non-USSPed as well as USSPed condition. Similar trend was found also for the samples exposed at 500 °C. It

is obvious from the data in Table 5.3 that the value of k_p is higher for the Type–1 salt sprayed samples exposed to 600 °C than for those sprayed with Type–2 and Type–3 salt mixtures. Further, k_p is higher for the non-USSPed condition as compared to those of the USSPed ones for all the three types of salt sprayed samples, exposed to 600 °C.

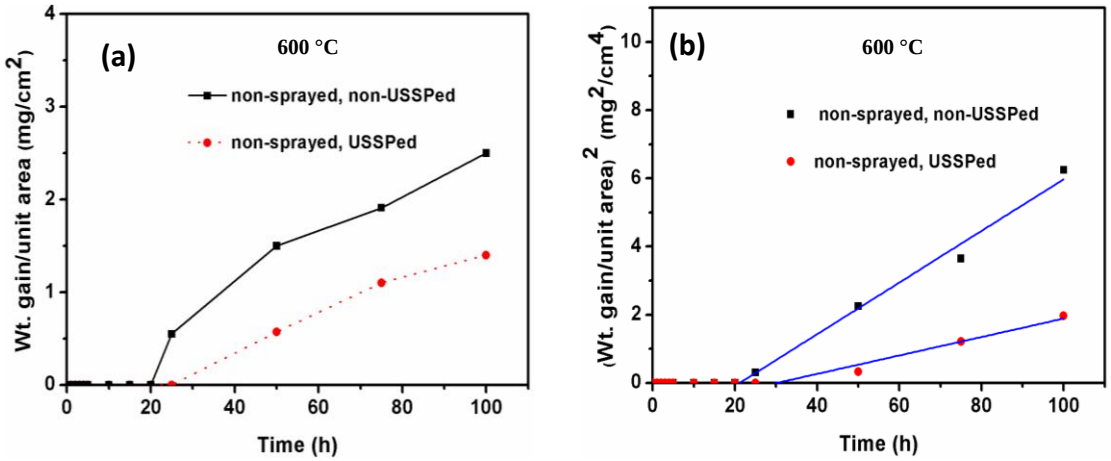

Fig. 5.11 Weight gain plots of non-sprayed samples for the non-USSPed and USSPed conditions, exposed at 600 °C up to 100h: (a) weight gain per unit area vs time of exposure, (b) square of weight gain per unit area vs time of exposure.

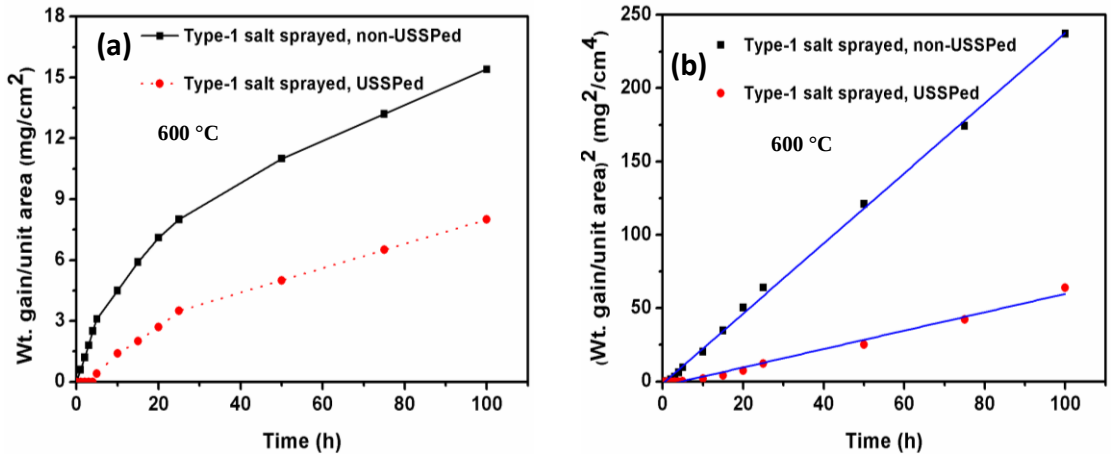

Fig. 5.12 Weight gain plots of Type–1 salt sprayed samples for the non-USSPed and USSPed conditions, exposed at 600 °C up to 100h: (a) weight gain per unit area vs time of exposure, (b) square of weight gain per unit area vs time of exposure.

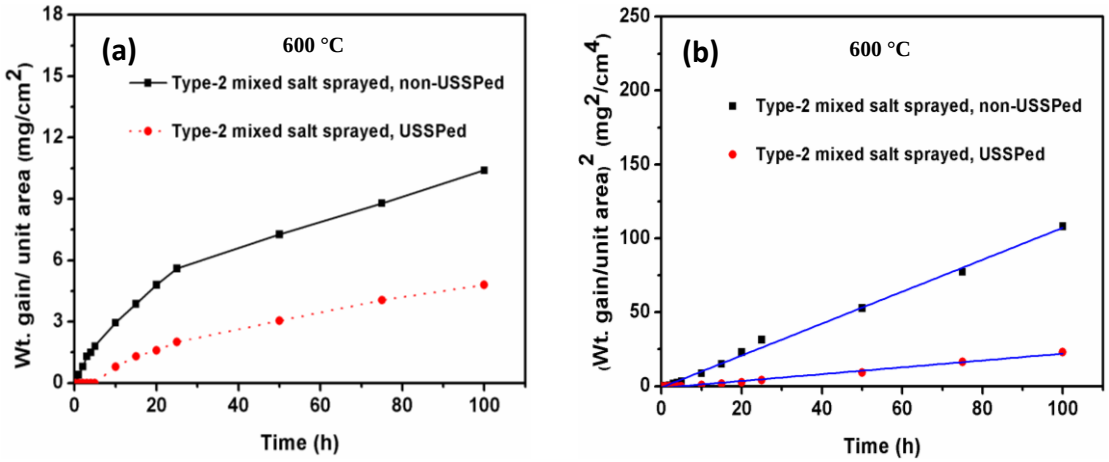

Fig. 5.13 Weight gain plots of Type–2 mixed salts sprayed samples for the non-USSPed and USSPed conditions, exposed at 600 °C up to 100h: (a) weight gain per unit area vs time of exposure, (b) square of weight gain per unit area vs time of exposure.

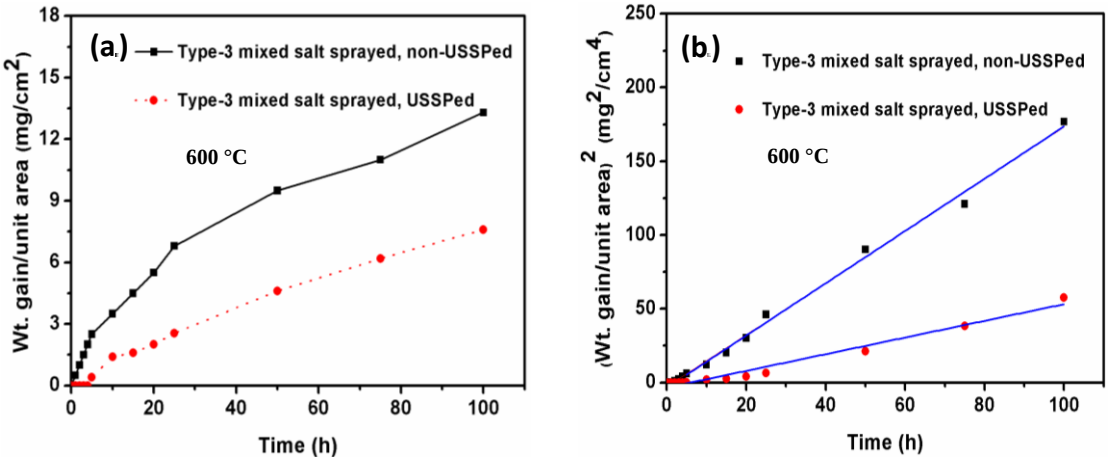

Fig. 5.14 Weight gain plots of Type–3 mixed salts sprayed samples for the non-USSPed and USSPed conditions, exposed at 600°C up to 100h: (a) weight gain per unit area vs time of exposure, (b) square of weight gain per unit area vs time of exposure.

Table 5.3 Parabolic rate constant (k_p) of the samples hot corroded at 600 °C for 100h.

Material condition	Type–1 salt sprayed		Type–2 mixed salts sprayed		Type–3 mixed salts sprayed	
	$k_p(mg^2cm^{-4}h^{-1})$	R^2	$k_p(mg^2cm^{-4}h^{-1})$	R^2	$k_p(mg^2cm^{-4}h^{-1})$	R^2
non-USSPed	245.8668	0.98	12.0918	0.99	57.2730	0.99
USSPed	4.2589	0.98	1.7029	0.99	3.670	0.97

5.4 CHARACTERIZATION OF CORROSION PRODUCTS

5.4.1 X-ray Diffraction Analysis

The various oxide products formed on hot corroded non-USSPed and USSPed specimens were characterized by XRD. The peaks of XRD for the non-USSPed as well as USSPed conditions, following hot corrosion at 500 and 600 °C for 100h, are shown in Figs. 5.15 and 5.16 respectively.

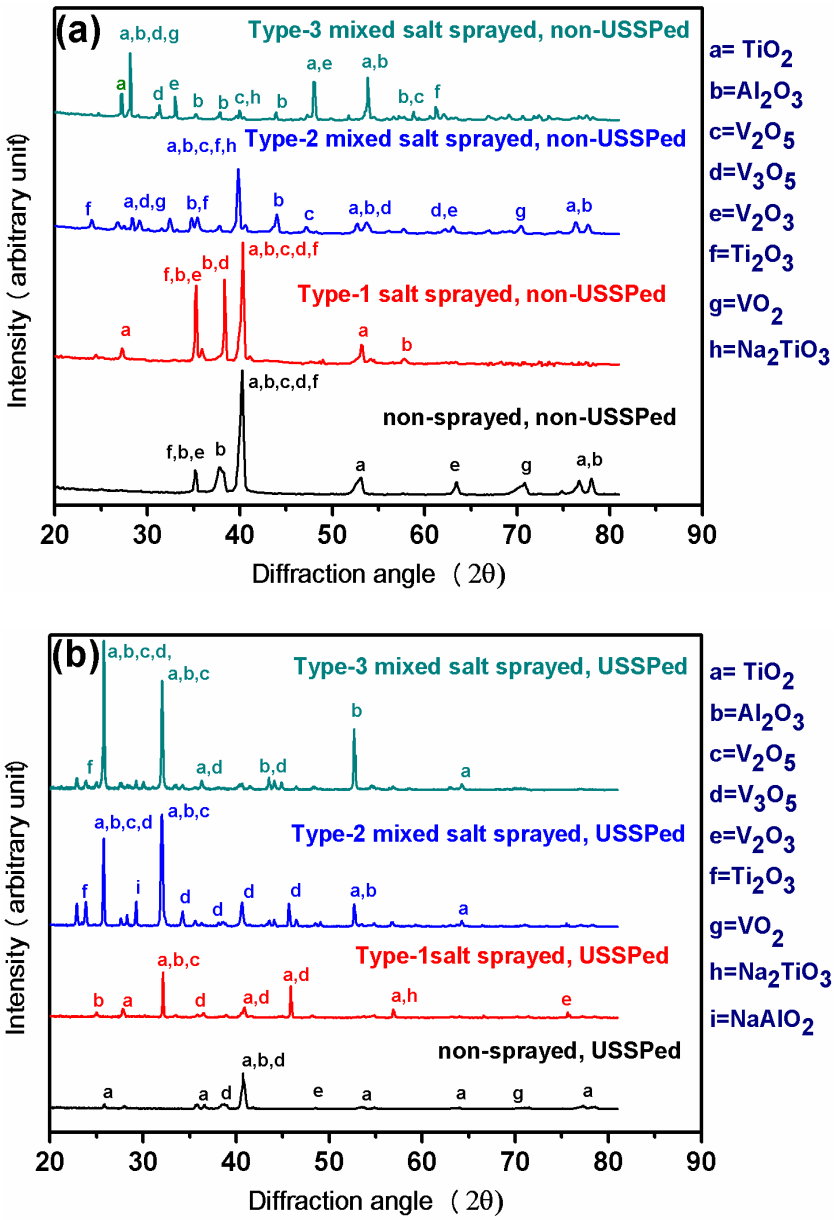

Fig. 5.15 XRD analysis of the non-sprayed and different salt/mixed salts prayed samples, exposed at 500 °C for 100h; (a) non-USSPed (b) USSPed.

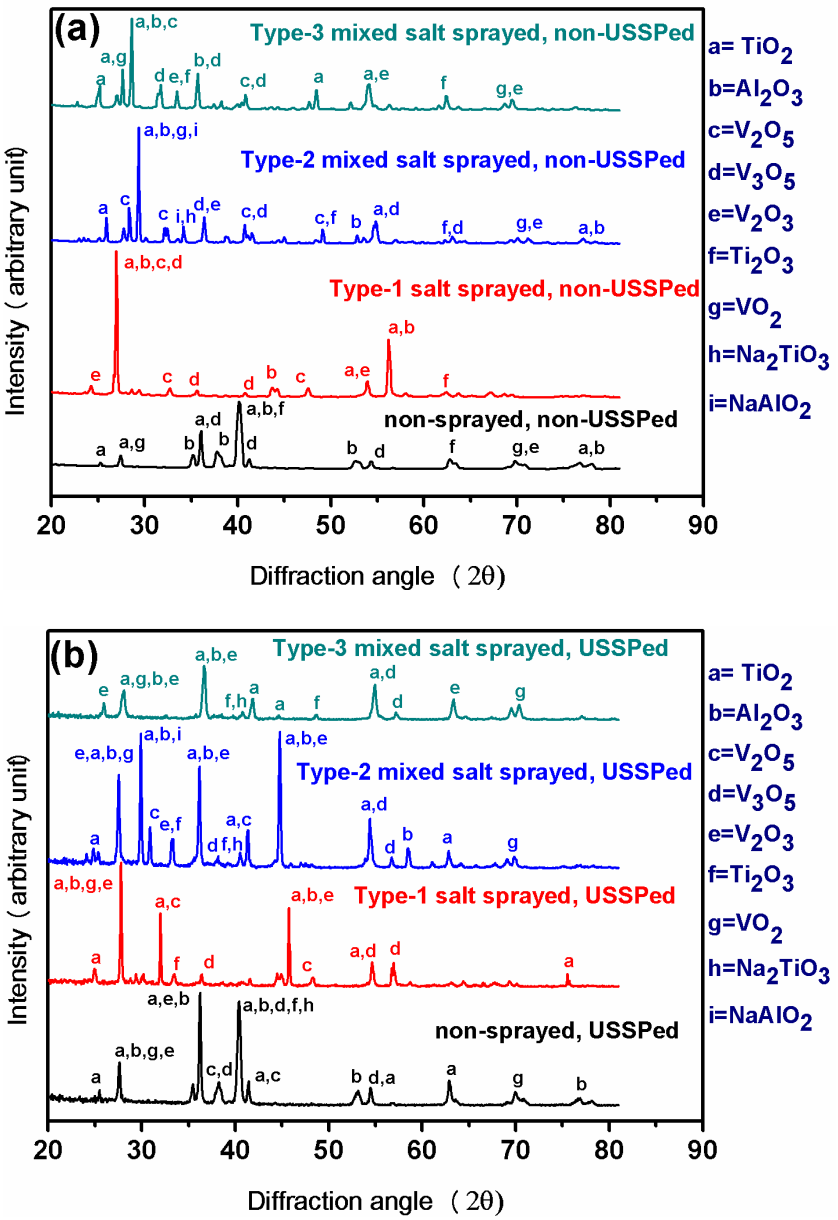

Fig. 5.16 XRD analysis of the non-sprayed and different salt/mixed salts sprayed samples, exposed at 600 °C for 100h; (a) non-USSPed (b) USSPed.

The corrosion products TiO_2, Al_2O_3, V_2O_3, Ti_2O_3, V_2O_5, VO_2, V_3O_5, $NaAlO_2$ and Na_2TiO_3 were observed, resulting from exposure at 500 and 600 °C for 100h.

The several compounds formed from hot corrosion in various conditions are listed in Table 5.4 (a, b). The change in Gibbs free energy *(ΔG°)* for the reactions to

form main oxides was used to explain relative stability of the formed oxides [David et al. (2009), Morita et al. (2003), Shreir et al. (2000)].

The values of $\Delta G°$ for the different oxides formed at 600 °C (presented as per mole of oxygen) for the formation of oxides are shown in Table 5.5. It may be seen from the data of Table 5.5 that the three oxides i.e. Al_2O_3, Ti_2O_3 and TiO_2 have significantly lower values of $\Delta G°$, -935, -930 and -752 kJ/mol respectively, compared to the other oxides. These thermodynamic data suggest that these oxides are more stable in comparison to the other oxides, recorded in Table 5.5.

Table 5.4a Oxides formed from hot corrosion of non-USSPed material, characterized by XRD.

Type of spray	**Corrosion products on non-USSPed samples exposed for 100h at:**	
	500 ºC	**600 ºC**
non-sprayed	TiO_2, Al_2O_3, V_2O_5, Ti_2O_3, V_3O_5, VO_2, V_2O_3	TiO_2, Al_2O_3, Ti_2O_3, V_3O_5, VO_2, V_2O_3
Type-1 salt sprayed	TiO_2, Al_2O_3, V_2O_3, V_3O_5, Ti_2O_3	TiO_2, Al_2O_3, V_2O_5, Ti_2O_3, V_3O_5, V_2O
Type-2 mixed salts sprayed	TiO_2, Al_2O_3, V_2O_5, V_3O_5, Ti_2O_3, Na_2TiO_3, VO_2, V_2O_3	TiO_2, Al_2O_3, V_2O_5, Ti_2O_3, VO_2, V_3O_5, V_2O_3, $NaAlO_2$, Na_2TiO_3
Type-3 mixed salts sprayed	TiO_2, Al_2O_3, V_2O_5, Ti_2O_3, Na_2TiO_3, VO_2, V_2O_3, V_3O_5	TiO_2, Al_2O_3, V_2O_5, VO_2, V_3O_5, V_2O_3, Ti_2O_3

Table 5.4b Oxides formed from hot corrosion of USSPed material, characterized by XRD.

Type of spray	**Corrosion products on USSPed samples exposed for 100h at:**	
	500 ºC	**600 ºC**
non- sprayed	TiO_2, Al_2O_3,V_3O_5, VO_2, V_2O_3	TiO_2, Al_2O_3, V_2O_5,V_2O_3, V_3O_5, Ti_2O_3, VO_2
Type-1 salt sprayed	TiO_2, Al_2O_3, V_2O_5, V_3O_5, V_2O_3,	TiO_2, Al_2O_3, V_2O_5,V_2O_3,VO_2, V_3O_5, Ti_2O_3
Type-2 mixed salts sprayed	TiO_2, Al_2O_3, V_2O_5, V_3O_5, Ti_2O_3, $NaAlO_2$	TiO_2, Al_2O_3, V_2O_5, V_2O_3, VO_2, V_3O_5, Ti_2O_3, Na_2TiO_3, $NaAlO_2$
Type-3 mixed salts sprayed	TiO_2, Al_2O_3, V_2O_5, V_3O_5,Ti_2O_3	TiO_2, Al_2O_3, VO_2, V_2O_3, V_3O_5, Ti_2O_3

Table 5.5 Gibbs free energy ($\Delta G°$) of formation of the main oxide products, per mole of oxygen, at 600 °C.

S. No.	**Oxide product**	**ΔG° (kJ/mol)**	**Reference**
1.	Al_2O_3	*-935*	Shreir et al. (2000)
2.	Ti_2O_3	*-930*	Morita et al. (2003)
3.	TiO_2	*-752*	Shreir et al. (2000)
4.	V_2O_3	*-692*	Shreir et al. (2000)
5.	V_2O_5	*-461*	David (2009)

5.4.2 SEM/EDS Analysis

Surface morphologies of the hot corroded samples of non-USSPed and USSPed material were characterized by SEM. However, the confirmation of the various oxides formed from the hot corrosion was done by EDS analysis. EDS analysis of all the samples, both of non-USSPed as well as USSPed showed that TiO_2 and Al_2O_3 were main constituents of the oxide layer with small amounts of V_2O_5 and V_2O_3. Figures 5.17, 5.18 and 5.19 show SEM micrographs of corroded samples of the non-USSPed and USSPed samples for Type–1 salt, Type–2 mixed salts and Type–3 mixed salts exposed to 400 °C.

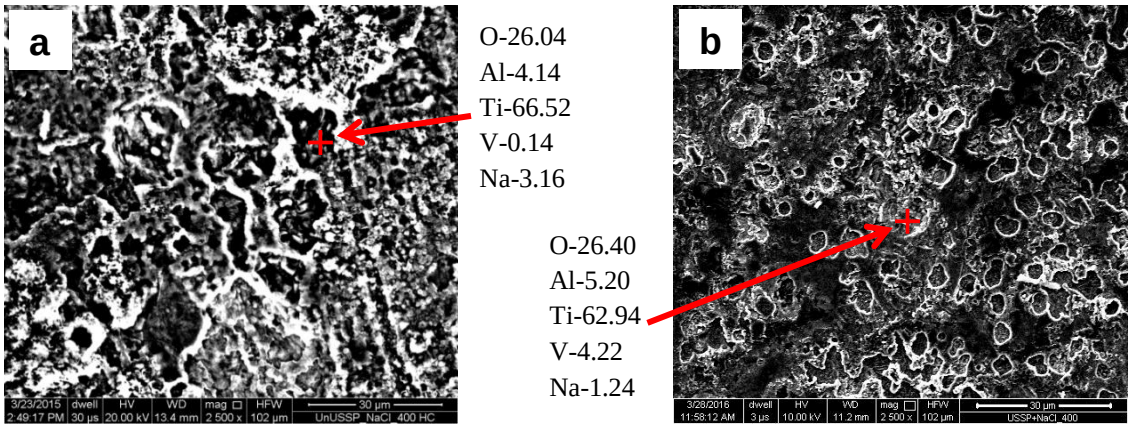

Fig. 5.17 SEM/EDS analysis of Type–1 salt (100% NaCl) sprayed samples exposed at 400 °C for 100h: (a) non-USSPed, (b) USSPed.

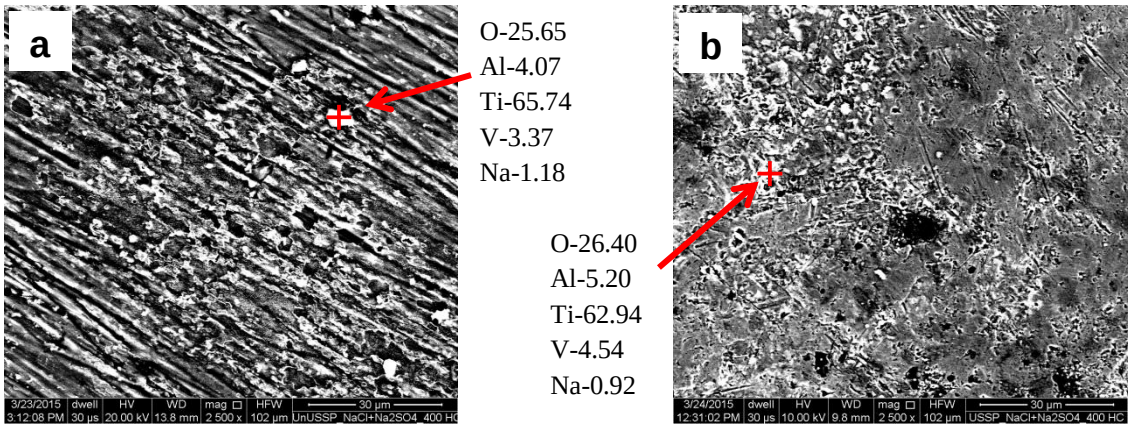

Fig. 5.18 SEM/EDS analysis of Type–2 mixed salts (75%Na_2SO_4+25% NaCl) sprayed samples exposed at 400 °C for 100h: (a) non-USSPed, (b) USSPed.

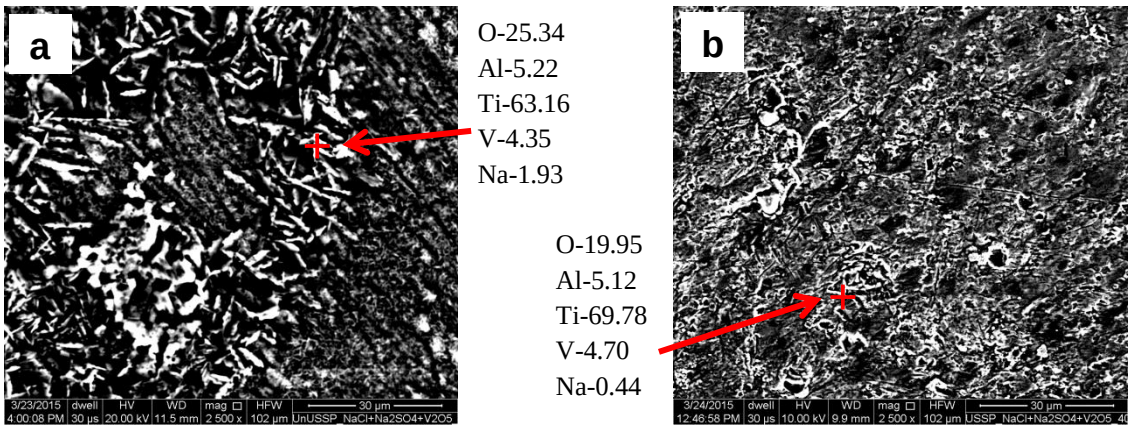

Fig. 5.19 SEM/EDS analysis of Type–3 mixed salts (90%Na_2SO_4+5%NaCl+5%V_2O_5) sprayed samples exposed at 400 ^oC for 100h: (a) non- USSPed, (b) USSPed.

SEM micrographs of the corroded samples from exposure at 500 °C showed spalling of oxide scale. The oxide scale formed from exposure at 500 °C up to 100h, was found cracked on the surface of the samples sprayed with Type–1 salt (100%NaCl), both in the non-USSPed as well as USSPed condition (Fig. 5.20). However, this type of behavior was not observed in the samples sprayed with the mixed salts spray of Type–2 and Type–3 (Figs. 5.21 and 5.22 respectively). Dry grass type oxide scale was found on the samples exposed to 500 °C in the Type–3 mixed salts sprayed samples in both the conditions (Fig. 5.22).

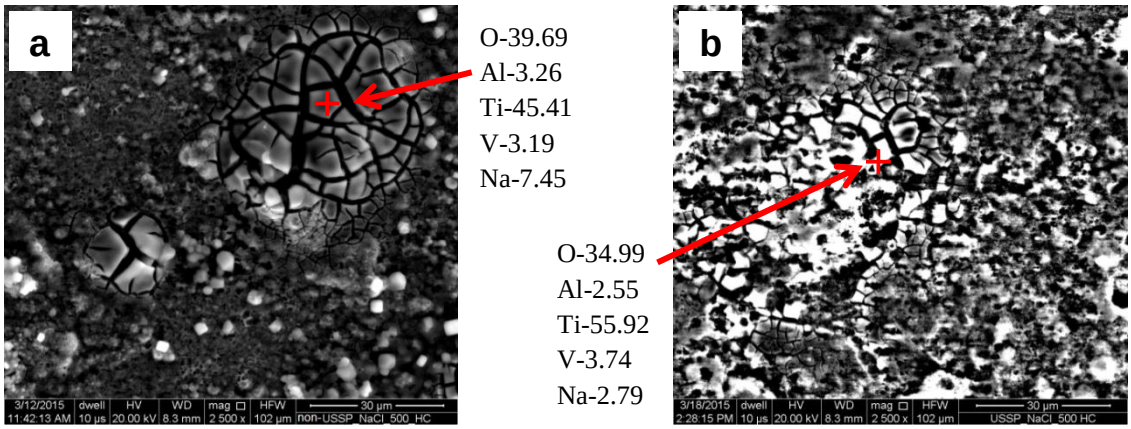

Fig. 5.20 SEM/EDS analysis of Type–1 salt (100% NaCl) sprayed samples exposed at 500 °C for 100h: (a) non-USSPed, (b) USSPed.

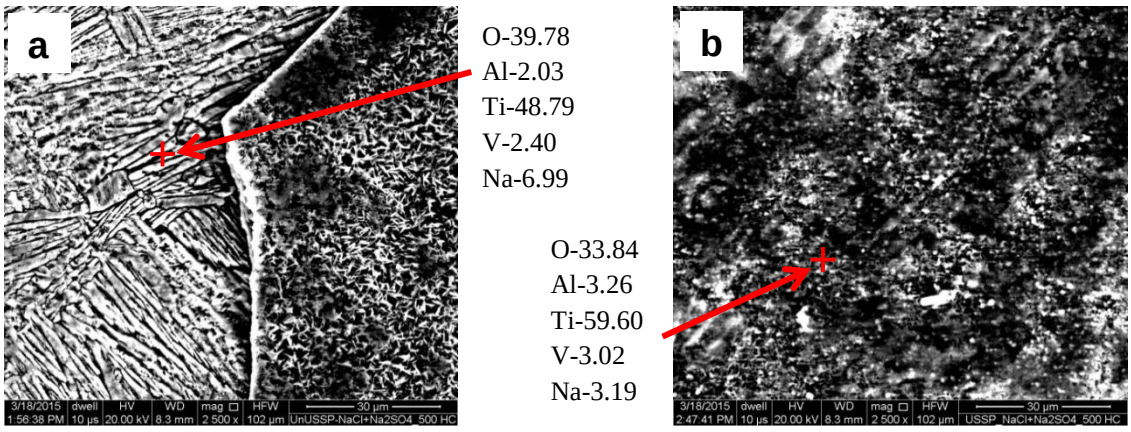

Fig. 5.21 SEM/EDS analysis of Type–2 mixed salts (75%Na_2SO_4+25% NaCl) sprayed samples, exposed at 500 ^oC for 100h: (a) non-USSPed, (b) USSPed.

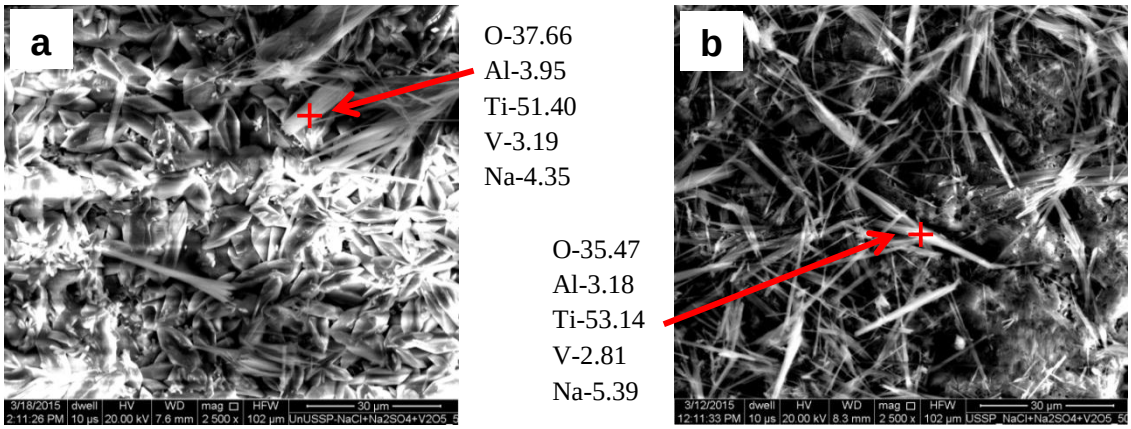

Fig. 5.22 SEM/EDS analysis of Type–3 mixed salts (90%Na_2SO_4+5%NaCl+5%V_2O_5) sprayed samples, exposed at 500 ^oC for 100h: (a) non-USSPed, (b) USSPed.

The non-sprayed samples oxidized in air at 600 °C showed globular oxides in the both non-USSPed as well as USSPed condition (Fig. 5.23). The size of globular oxide was bigger in the USSPed sample. SEM micrographs of corroded samples from the exposure at 600 °C up to 100h, sprayed with Type–1 salt, Type–2 and Type–3 mixed salts, in both the non-USSPed as well as USSPed condition are shown in Figs. 5.24-5.26. It may be seen from the micrographs of the hot corroded samples that salt attack was non-uniform.

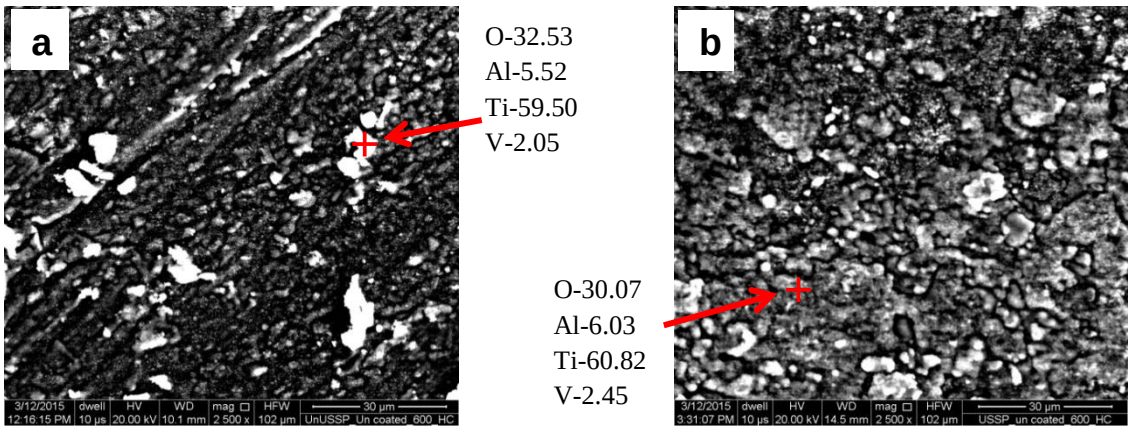

Fig. 5.23 SEM/EDS analysis of non-sprayed samples, exposed at 600 °C for100h: (a) non-USSPed, (b) USSPed.

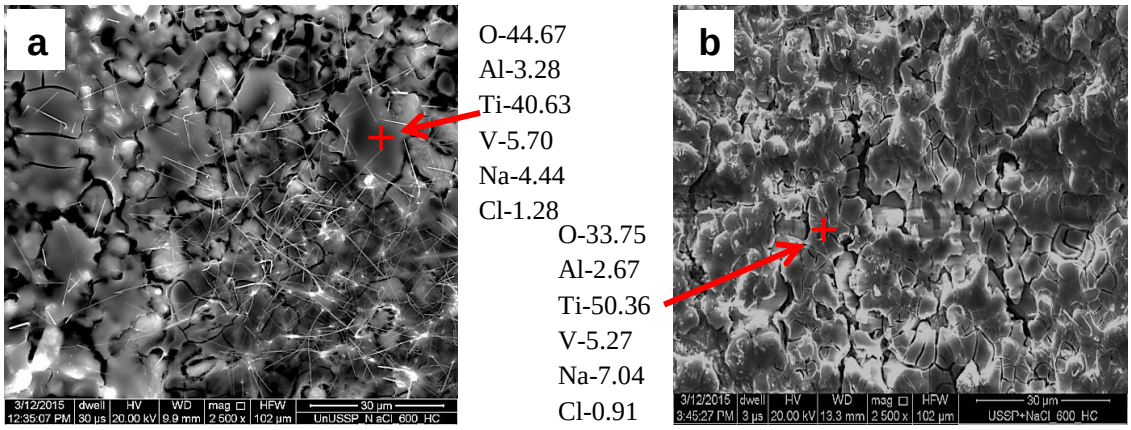

Fig. 5.24 SEM/EDS analysis of Type–1 salt (100% NaCl) sprayed samples, exposed at 600 °C for 100h: (a) non-USSPed, (b) USSPed.

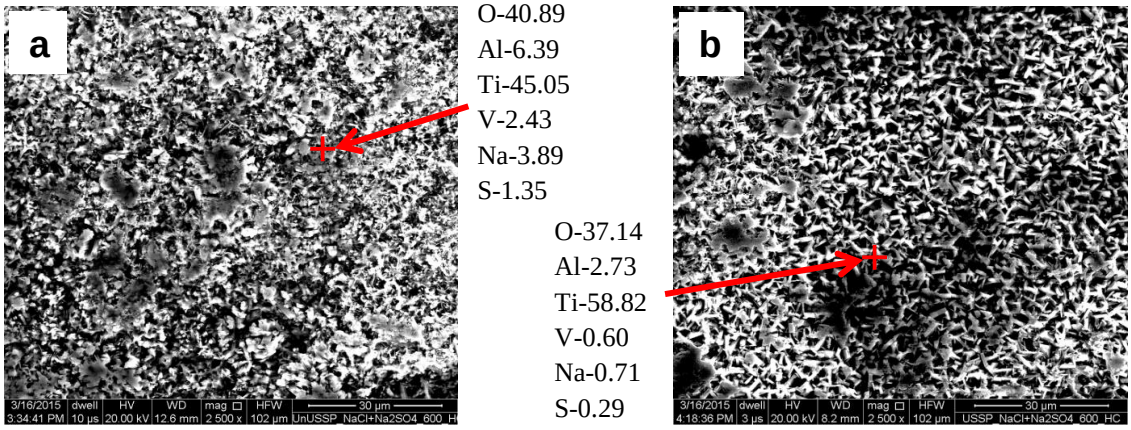

Fig. 5.25 SEM/EDS analysis of Type–2 mixed salts (75%Na_2SO_4+25% NaCl) sprayed samples, exposed at 600 ^{o}C for 100h: (a) non-USSPed, (b) USSPed.

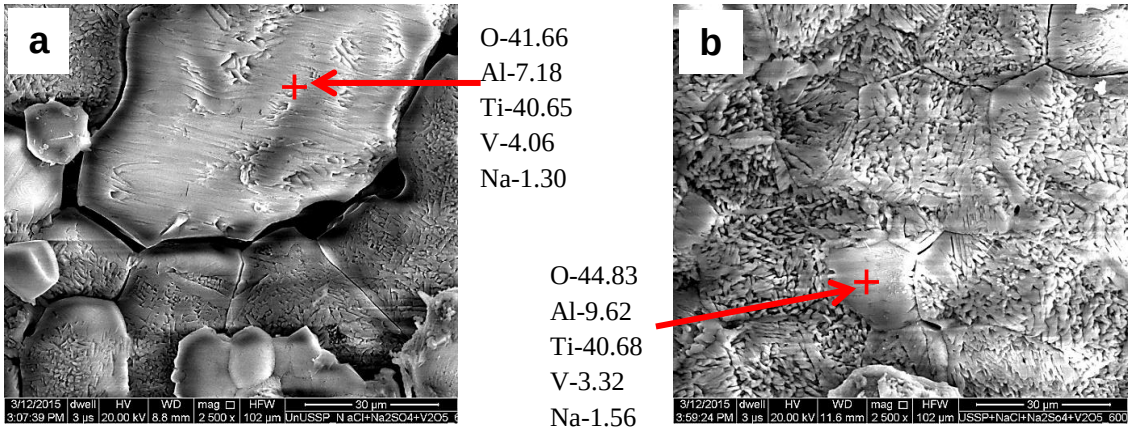

Fig. 5.26 SEM/EDS analysis of Type–3 mixed salts (90%Na_2SO_4+ 5%NaCl+5%V_2O_5) sprayed samples, exposed at 600 ^{0}C for 100h: (a) non-USSPed, (b) USSPed.

The cracking of oxide scale also resulted from exposure at 600 °C up to 100h, on the samples salt sprayed with Type–1 (100%NaCl), both in the non-USSPed as well as USSPed condition (Fig. 5.24). Relatively larger cracks were seen on the USSPed surface (Fig. 24a). Type–3 mixed salts (90%Na_2SO_4+5%NaCl+5%V_2O_5) sprayed samples exhibited wheat grain features of oxide layer (Fig. 5.26) and were found cracked on the surface.

5.4.3 SEM/EDS Examination of Sectioned Hot Corroded Specimens

The non-sprayed and sprayed with salt/mixed salts samples were sectioned diametrically, perpendicular to the top exposed surface after 100h of exposure at 500 and 600 °C to check the thickness of oxide layer. There was no oxide layer in the non-sprayed samples for both the conditions (Fig. 5.27). However, oxide scale was formed on the non-USSPed as well as USSPed samples following spray of Type–1 salt, Type–2 mixed salts and Type–3 mixed salts, from exposure at 500 °C for 100h (Fig. 5.28). Thicker oxide layer was observed on the non-USSPed sample than that on the USSPed

samples following Type–1 salt, Type–2 and Type–3 mixed salts spray and exposed at 500 °C.

However, thicker oxide scale was formed on the USSPed specimen of the non-sprayed material, exposed to 600 °C for 100h due to undulations developed on the surface from USSP. It may be seen that two oxide layers are visible (inner and outer) in Fig. 5.29b for the USSPed sample. This type of oxide layer was not observed on the non-USSPed sample. It may be seen from Figs. 5.30-5.32 that thicker oxide scale formed on the non-USSPed specimens in comparison to those on the USSPed samples, sprayed with Type–1 salt, Type–2 mixed salts and Type–3 mixed salts and exposed at 600 °C for 100h. Similarly, two oxide layers are visible in Figs. 5.30b, 5.31b and 5.32b in the USSPed samples sprayed with salt/mixed salts and exposed at 600 °C. The point analysis shows that quantity of oxygen was decreased in the interior of both non-USSPed and USSPed samples. However, the quantity of oxygen was lower in the USSPed samples than that in the non-USSPed one.

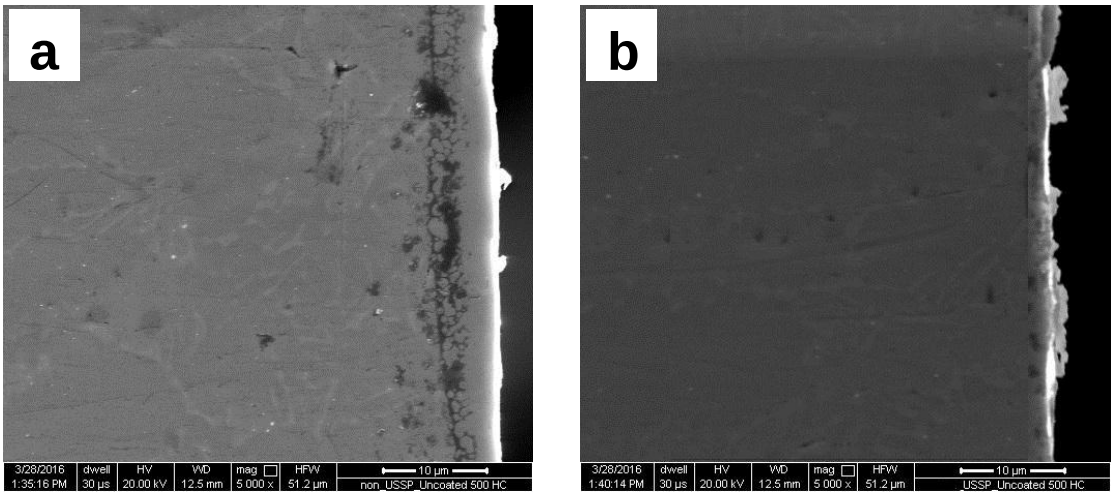

Fig. 5.27 Oxide scale morphology from surface towards interior across the thickness of the non-sprayed samples, subjected to hot corrosion for 100h at 500 °C: (a) non-USSPed (b) USSPed.

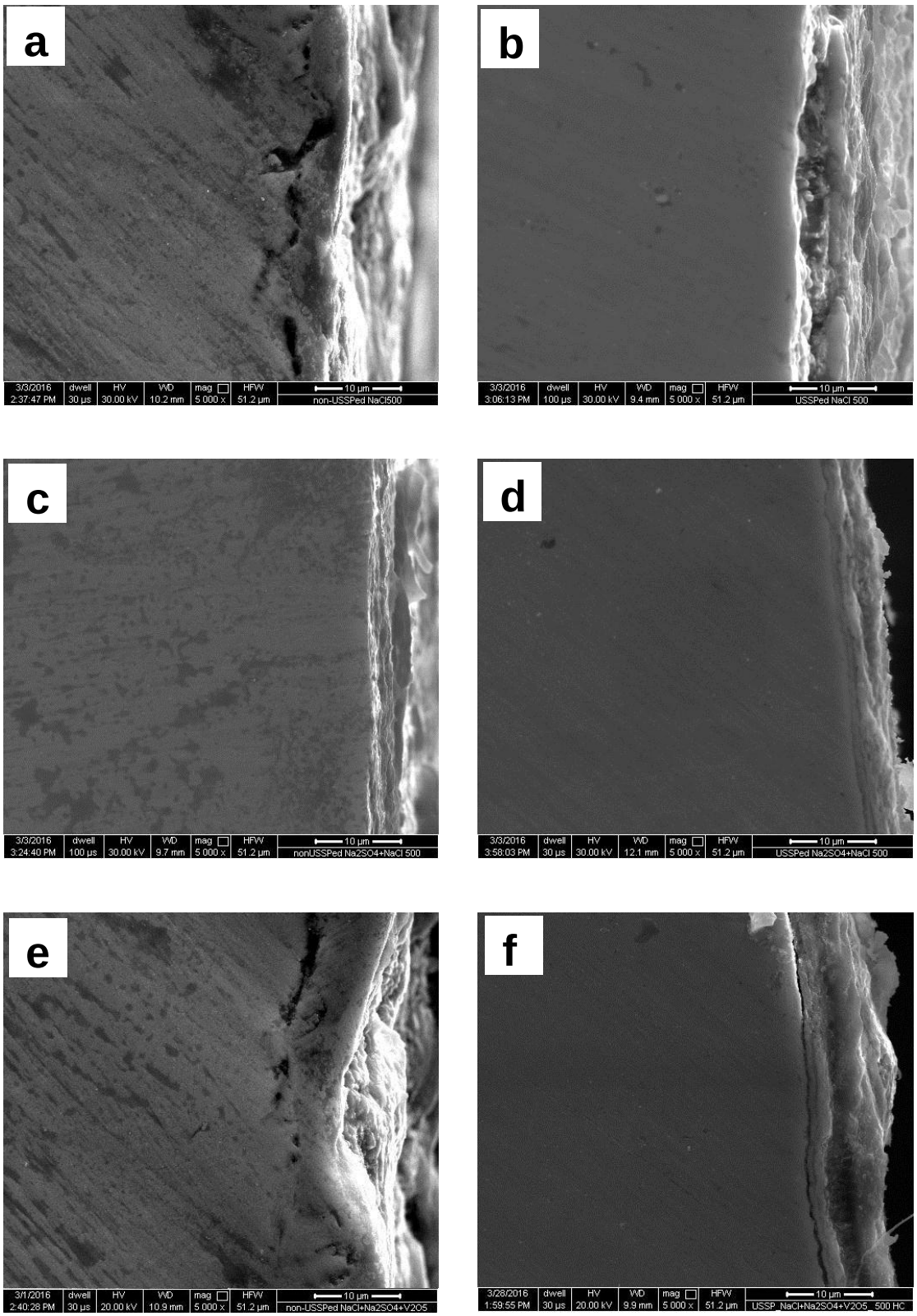

Fig. 5.28 Oxide scale morphology from surface towards interior across the thickness of the Type–1 salt sprayed (a, b), Type–2 mixed salts (c, d) and Type–3 (e, f) mixed salts sprayed samples, subjected to hot corrosion for 100h at 500 °C: non-USSPed (a, c, e) and USSPed (b, d, f).

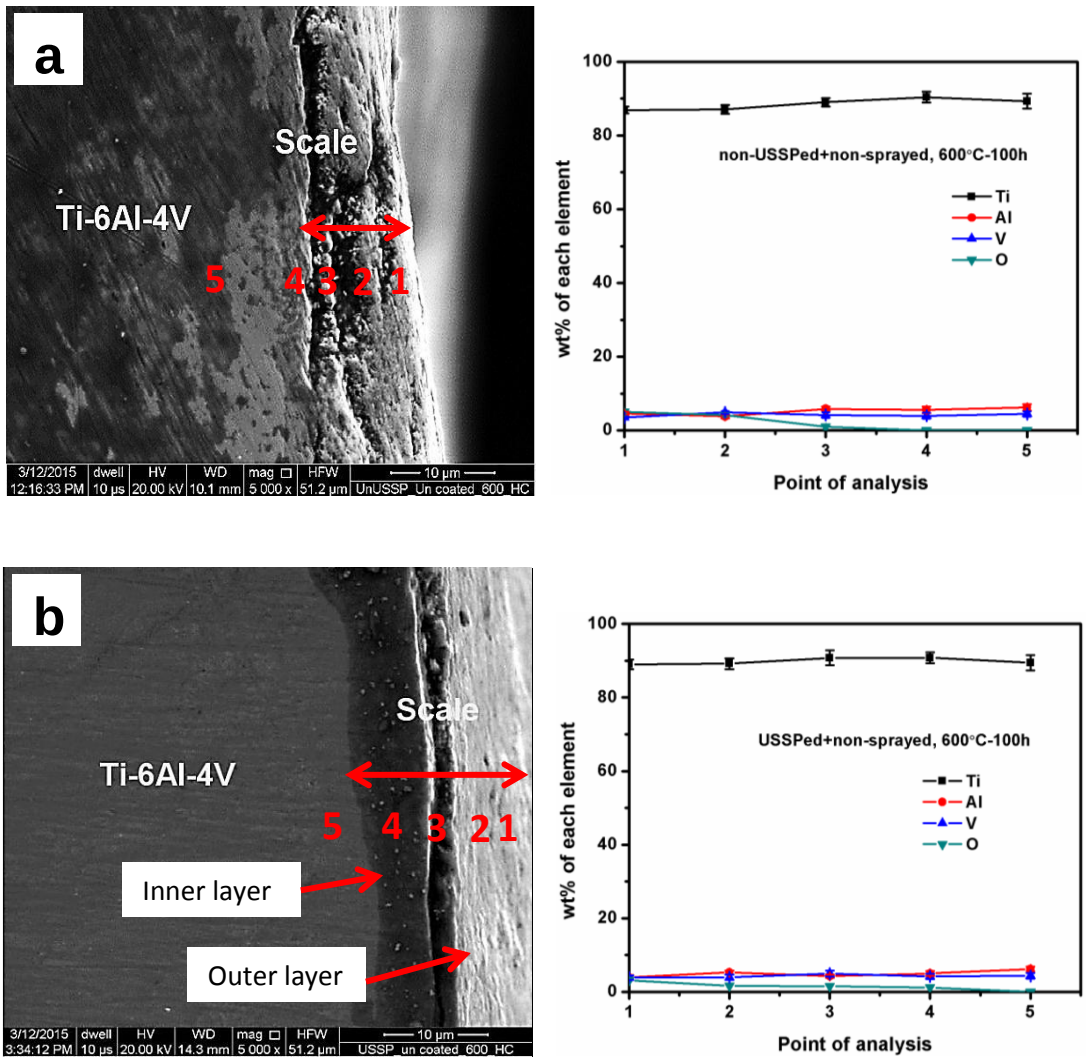

Fig. 5.29 Oxide scale morphology from surface towards interior across the thickness of the non-sprayed sample, subjected to hot corrosion for 100h at 600 °C: (a) non-USSPed (b) USSPed.

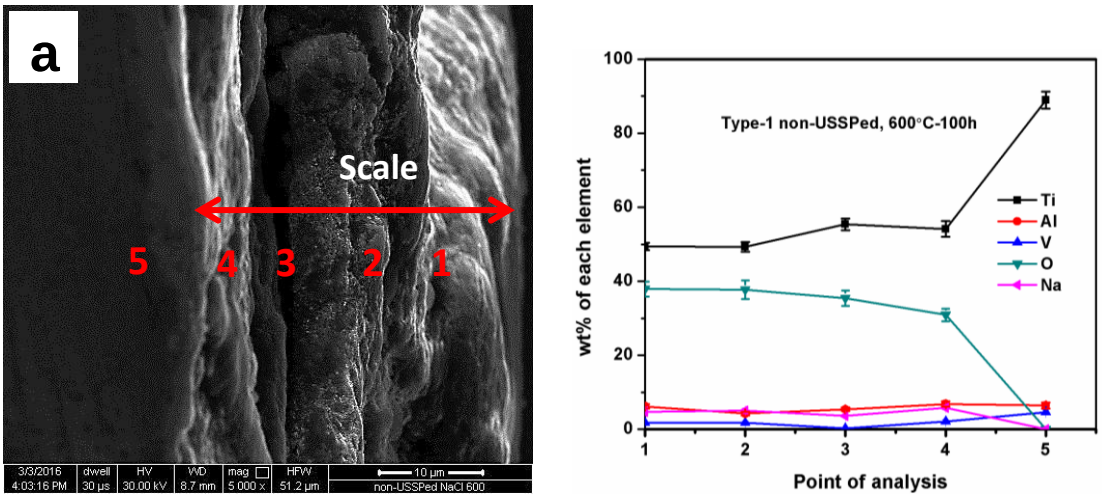

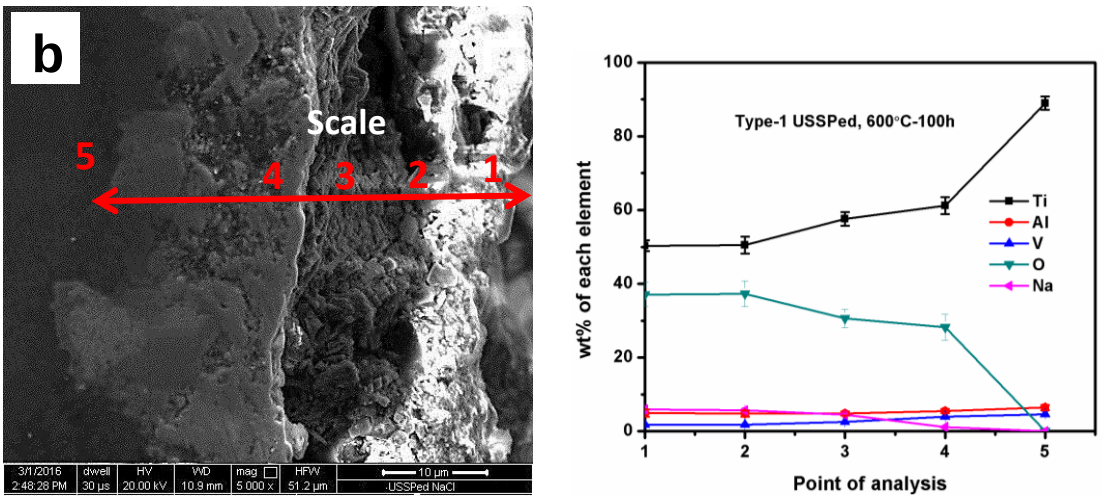

Fig. 5.30 Oxide scale morphology from surface towards interior across the thickness of the Type–1 salt sprayed, subjected to hot corrosion for 100h at 600 °C: (a) non-USSPed (b) USSPed.

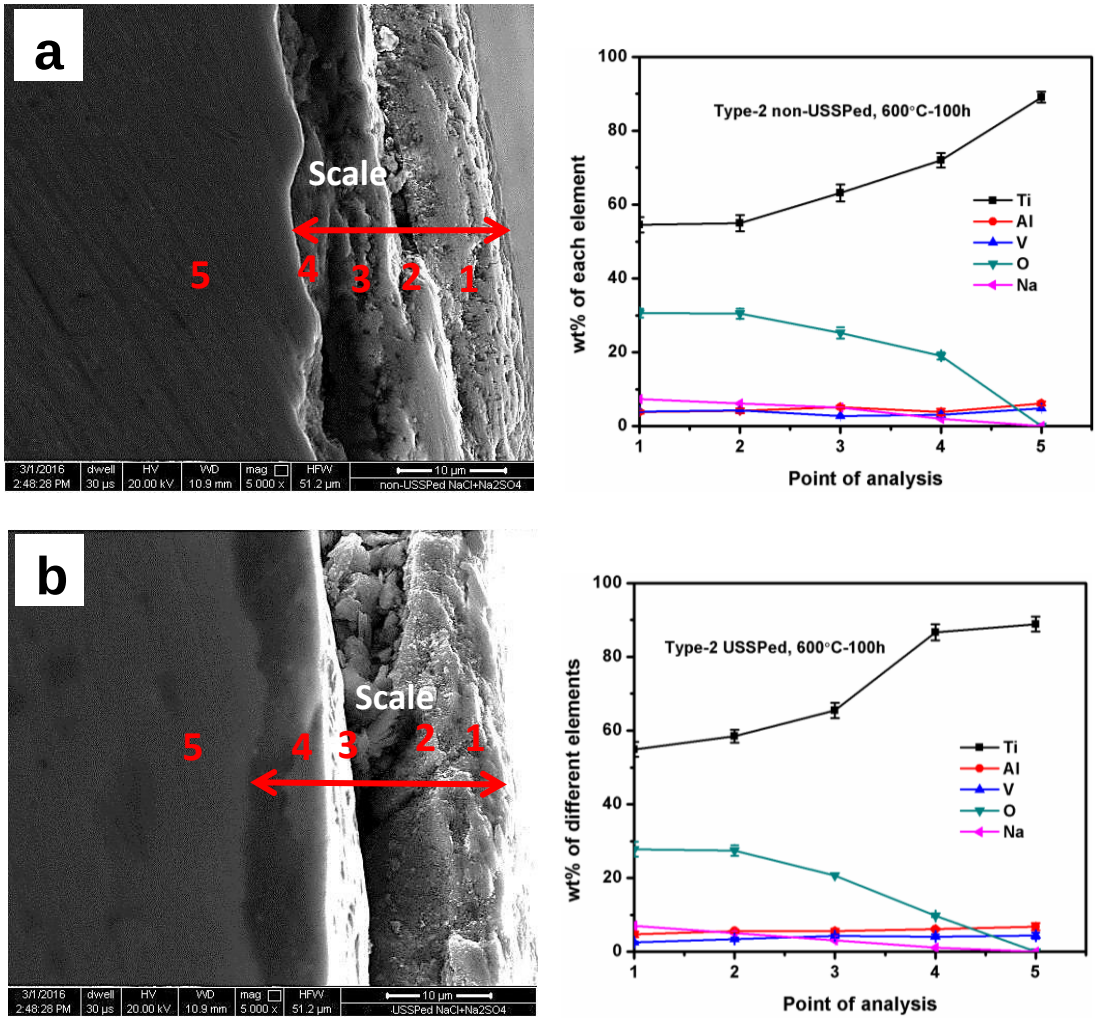

Fig. 5.31 Oxide scale morphology from surface towards interior across the thickness of the Type–2 mixed salts sprayed, subjected to hot corrosion for 100h at 600 °C: (a) non-USSPed (b) USSPed.

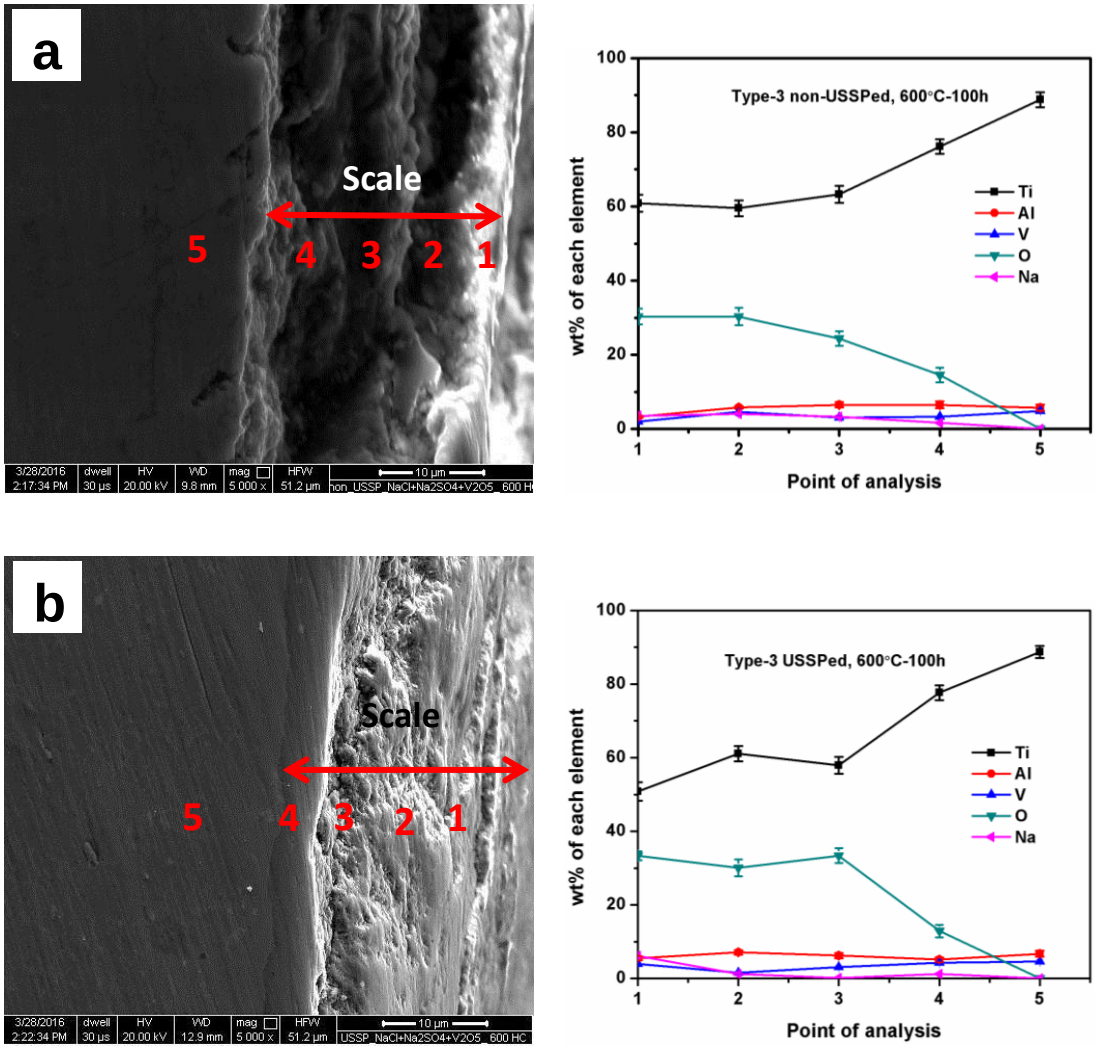

Fig. 5.32 Oxide scale morphology from surface towards interior across the thickness of the Type–3 mixed salts sprayed, subjected to hot corrosion for 100h at 600 °C: (a) non-USSPed (b) USSPed.

5.5 ELECTRON PROBE MICRO-ANALYSIS (EPMA) OF SECTIONED HOT CORRODED SPECIMENS

The elemental mapping of the corroded samples was carried out using wavelength dispersive spectroscopy (WDS). The corrosion resistance at 600 °C was found to be higher for Type–2 mixed salts sprayed samples in comparison to Type–1 salt and Type–3 mixed salts spray. Therefore, it was necessary to carry out EPMA analysis of the corroded samples. The elemental mapping of Type–1 salt, Type–2 mixed salts and Type–3 mixed salts sprayed samples in both the conditions, the non-USSPed and USSPed, sectioned perpendicular to corroded surface, following 100h of exposure at 600 °C, is shown in Figs. 5.33 to 5.40. It is important to mention that dense oxide scale was formed on USSPed sample, in agreement to the earlier observation made by Wen et al. (2012).

The elemental maps revealed variation of titanium, aluminium, vanadium, and oxygen in hot corroded samples of the both, non-USSPed and USSPed material. The diffusion of titanium, aluminium and vanadium, from the base material resulted in formation of TiO_2, Al_2O_3, V_2O_5, VO_2 and V_2O_3 oxides. Presence of titanium, aluminium, vanadium and oxygen in the surface region was revealed by X-ray mapping suggesting presence of various oxides layers formed in the both non-USSPed as well as USSPed material.

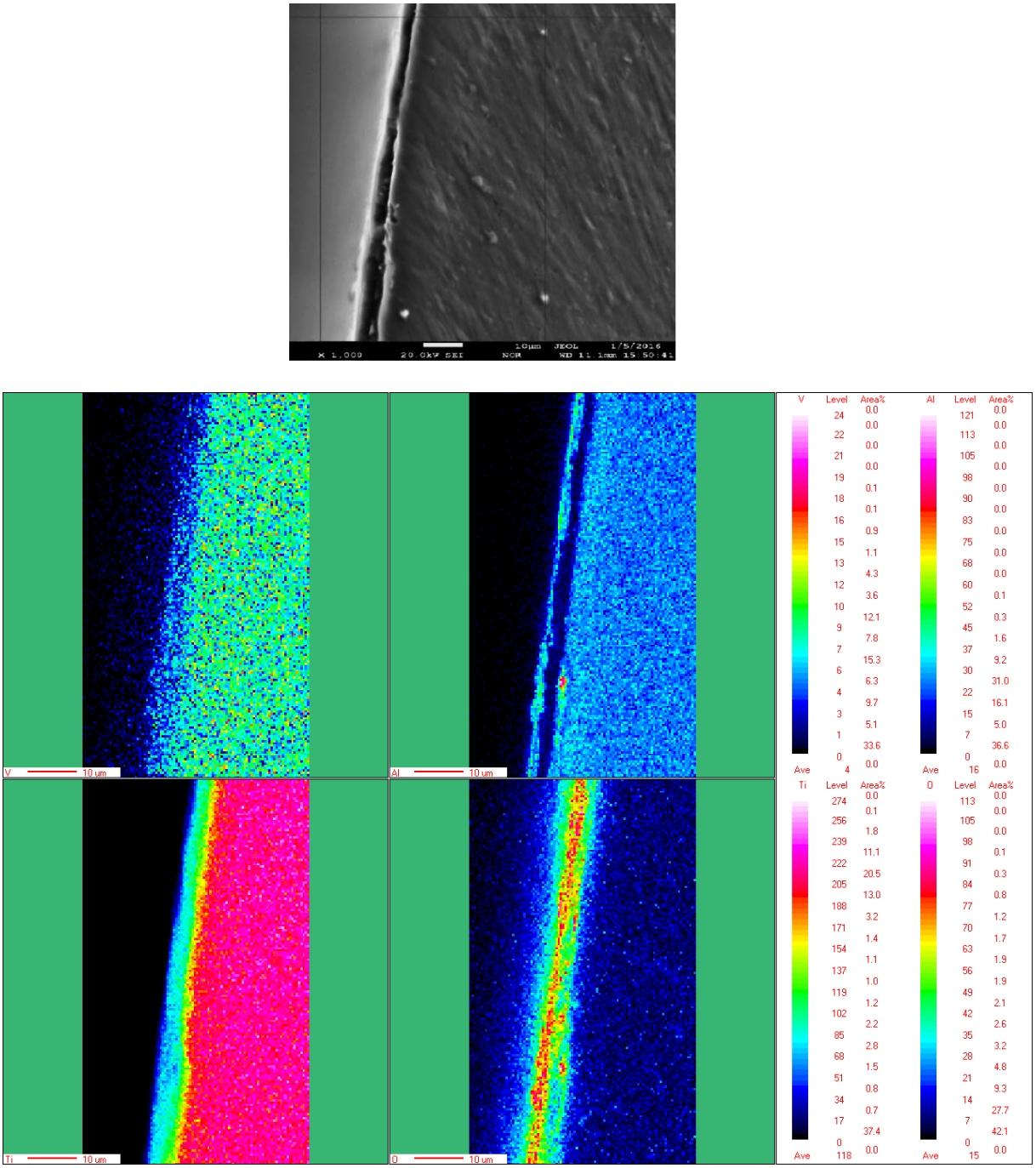

Fig. 5.33 X-ray mapping and variation of elemental concentration from surface towards interior across the thickness of the non-sprayed sample, subjected to hot corrosion for 100h at 600 °C for the non-USSPed sample.

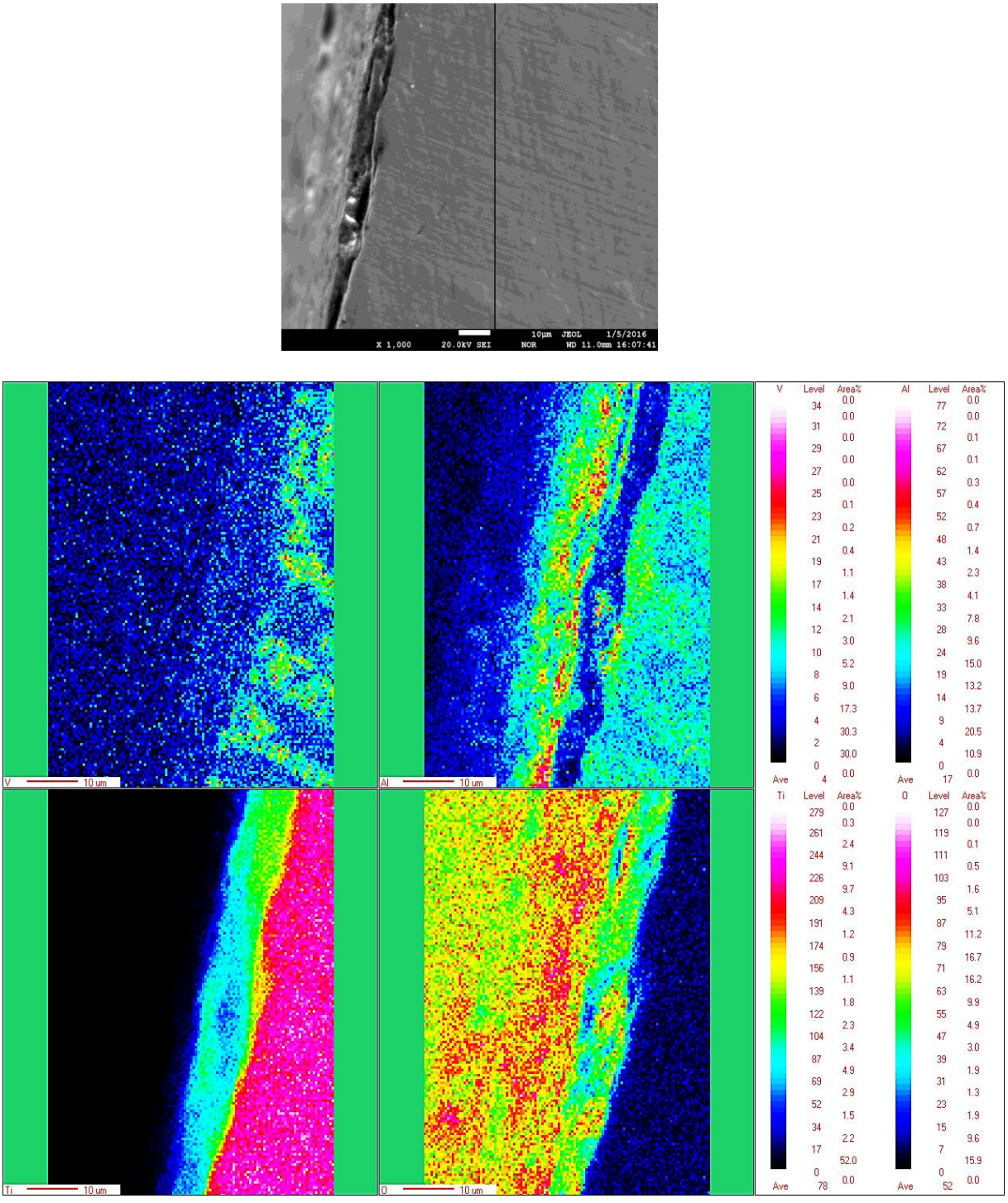

Fig. 5.34 X-ray mapping and variation of elemental concentration from surface towards interior across the thickness of the non-sprayed sample, subjected to hot corrosion for 100h at 600 °C for the USSPed sample.

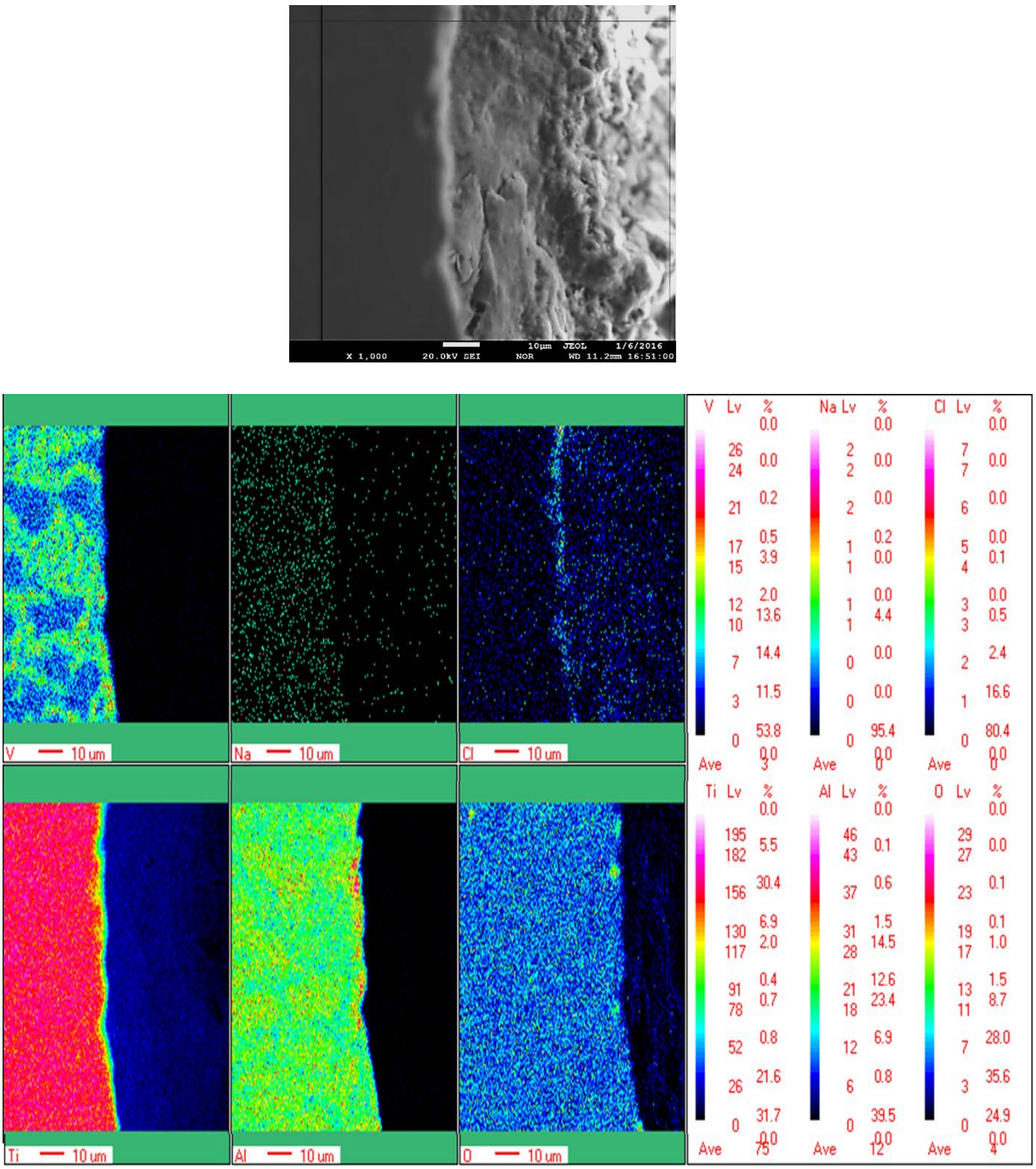

Fig. 5.35 X-ray mapping and variation of elemental concentration from surface towards interior across the thickness of the sample sprayed with Type-1 salt, subjected to hot corrosion for 100h at 600 °C for the non-USSPed sample.

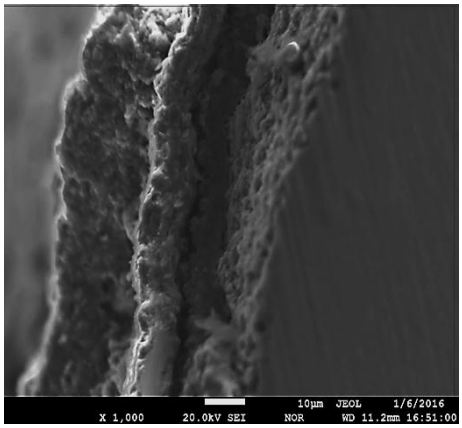

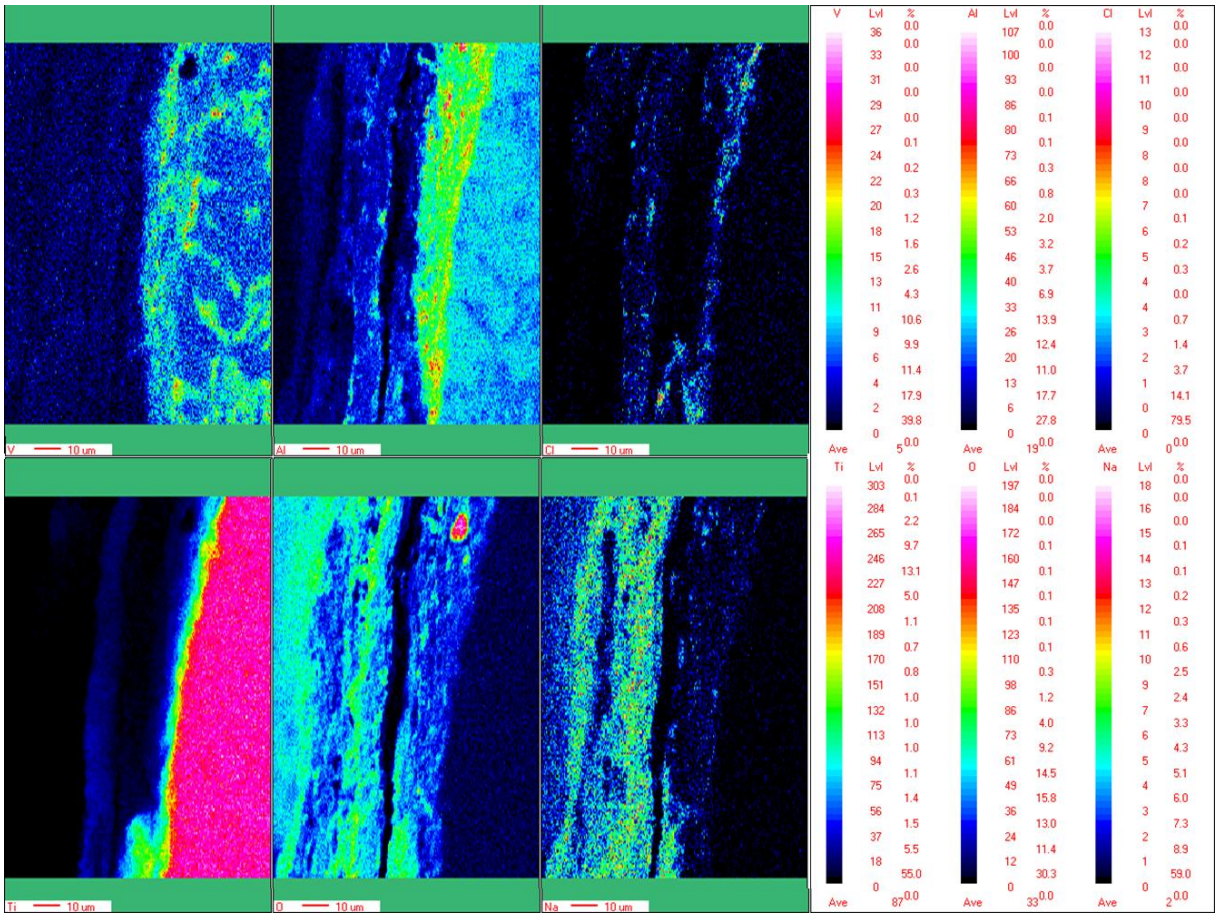

Fig. 5.36 X-ray mapping and variation of elemental concentration from surface towards interior across the thickness of the sample sprayed with Type-1 salt, subjected to hot corrosion for 100h at 600 °C for the USSPed sample.

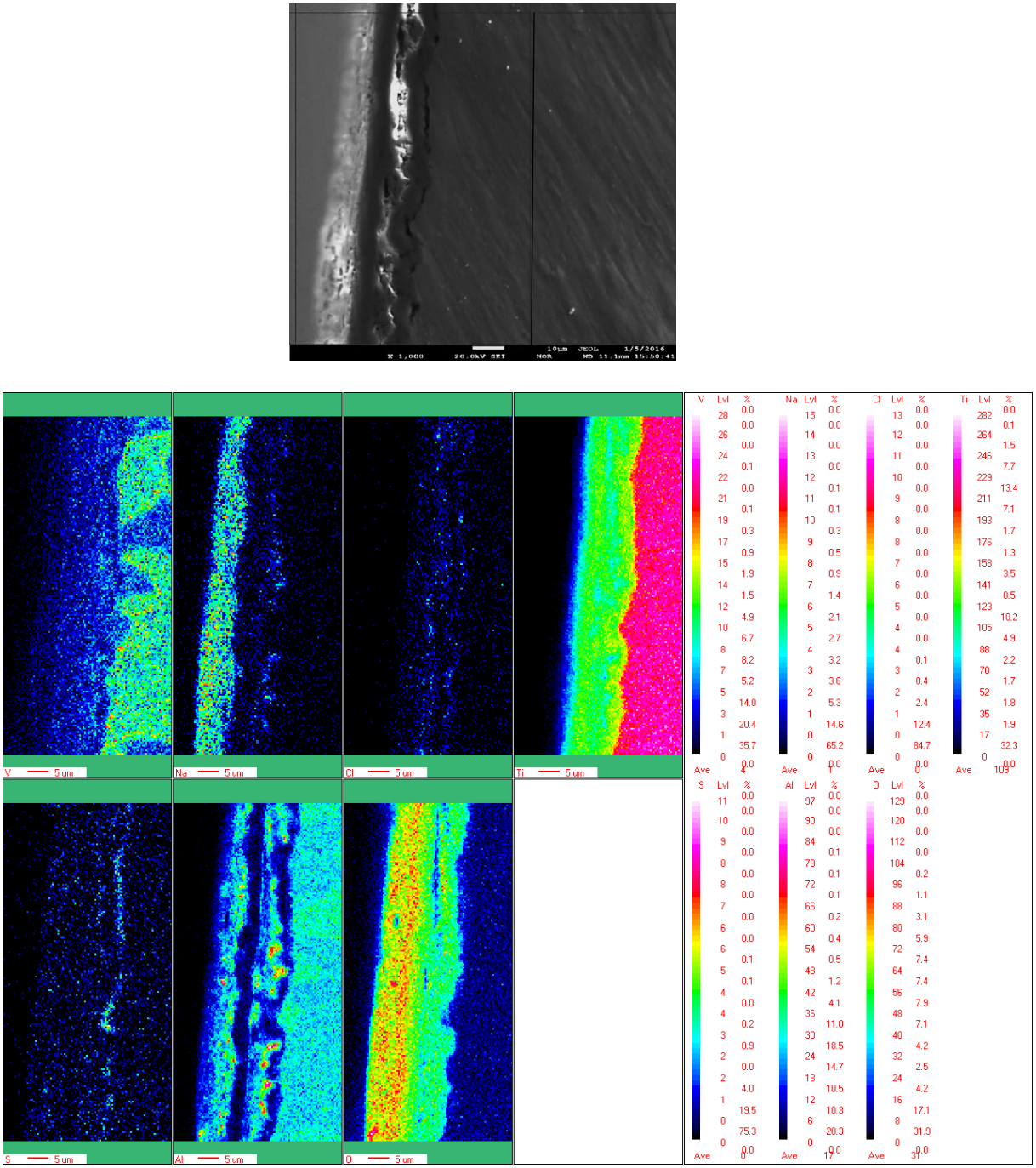

Fig. 5.37 X-ray mapping and variation of elemental concentration from surface towards interior across the thickness of the sample sprayed with Type–2 mixed salts, subjected to hot corrosion for 100h at 600 °C for the non-USSPed sample.

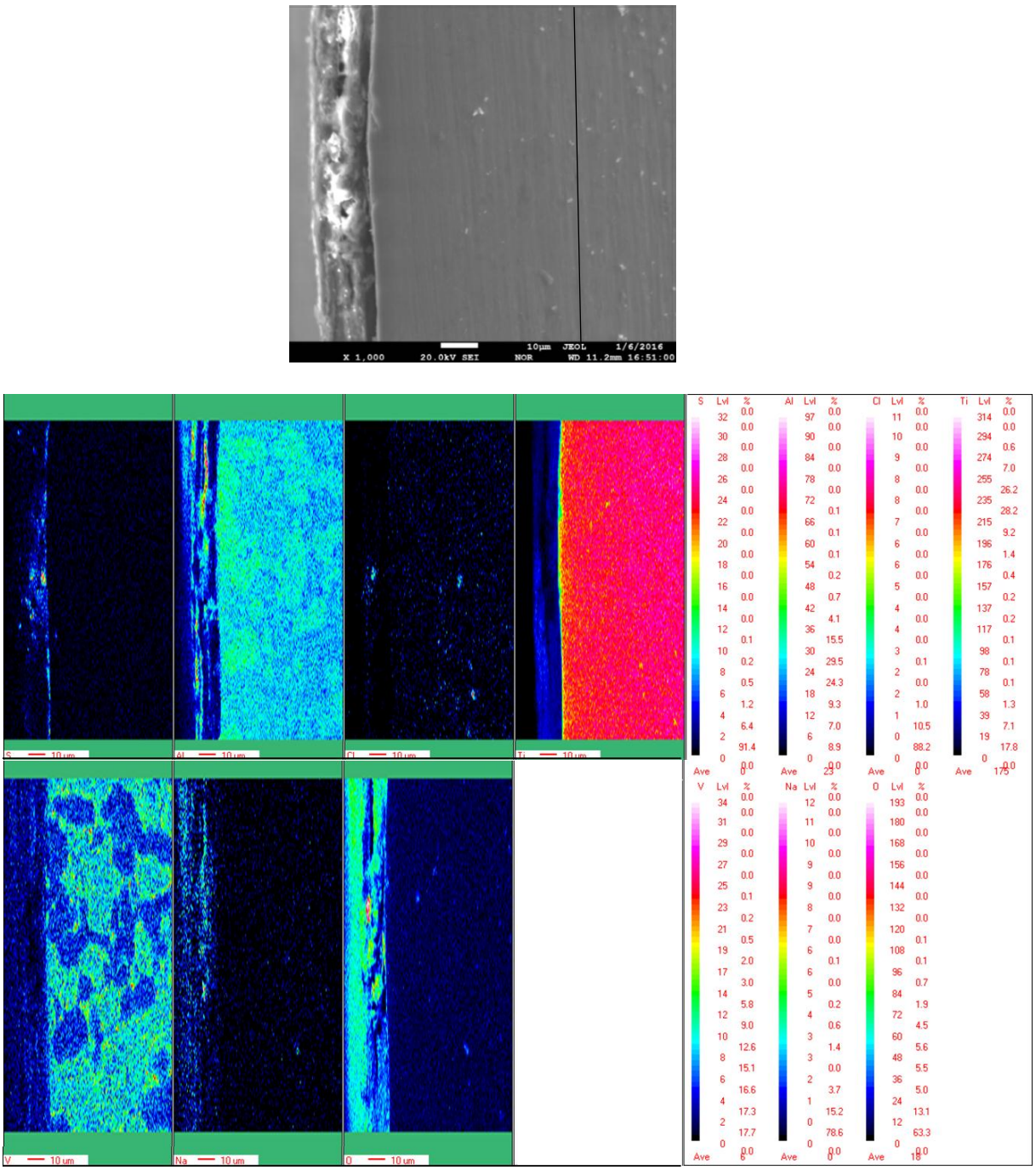

Fig. 5.38 X-ray mapping and variation of elemental concentration from surface towards interior across the thickness of the sample sprayed with Type–2 mixed salts, subjected to hot corrosion for 100h at 600 °C for the USSPed sample.

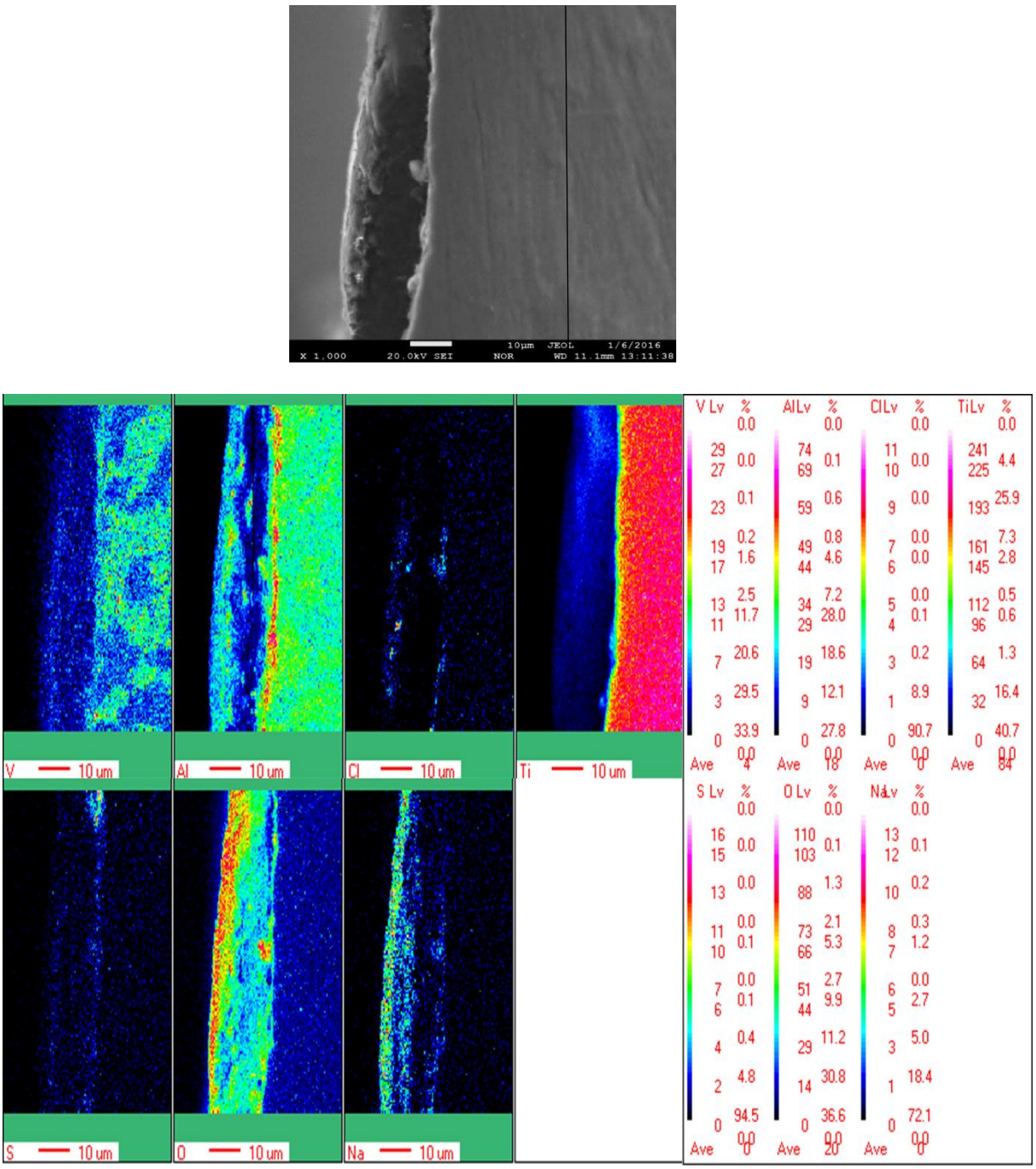

Fig. 5.39 X-ray mapping and variation of elemental concentration from surface towards interior across the thickness of the sample sprayed with Type–3 mixed salts, subjected to hot corrosion for 100h at 600 °C for the non-USSPed sample.

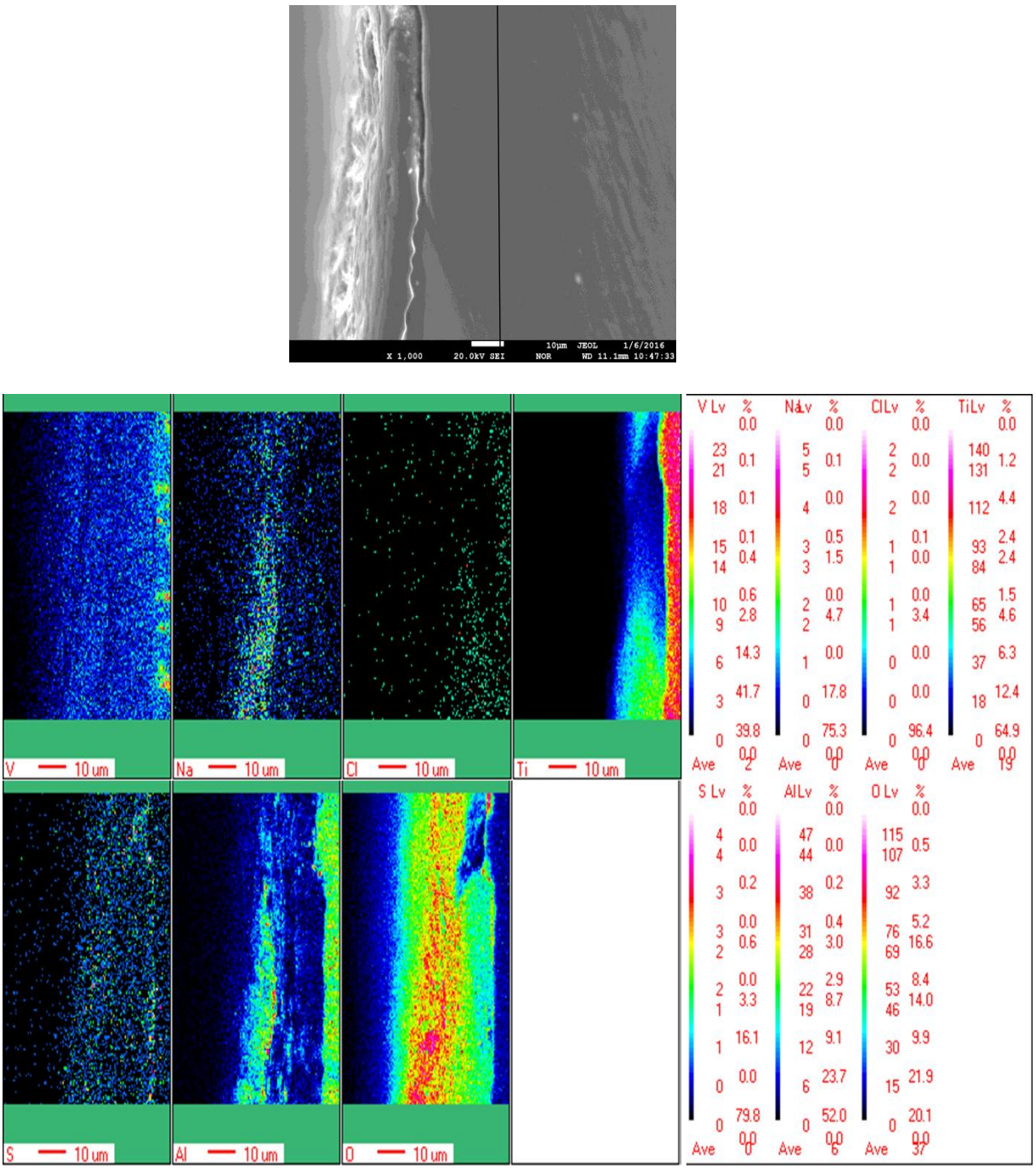

Fig. 5.40 X-ray mapping and variation of elemental concentration from surface towards interior across the thickness of the sample sprayed with Type–3 mixed salts, subjected to hot corrosion for 100h at 600 °C for the USSPed sample.

5.6 DISCUSSION

The visual observation of corroded samples shows that colour of the surface changed with the temperature of prior exposure (Figs 5.2-5.4). There was very thin oxide layer on the non-sprayed samples exposed at 400 and 500 °C and only minor changes were observed in weight of the salt sprayed samples exposed at 400 °C. However, significant changes were observed in the weights of the sprayed samples, exposed at 600 °C than in those exposed at 500 °C, up to 100h. In general, corrosion kinetics of the USSPed samples was found to be slower than those of the non-USSPed ones. Also, the weight gain per unit area and k_p values were relatively less in the samples subjected to USSP (Tables 5.1, 5.2 and 5.3).

Weight gain per unit area vs time of exposure plot showed that there was almost no change in weight during the first 5h in the USSPed samples since self-diffusion of ions was sluggish at initial stage of hot corrosion (Figs 5.5-5.15). However, there was no change in the weight up to 20h in the non-sprayed sample from exposure at 600 °C. The XRD peaks for the both, non-USSPed and USSPed corroded samples, exposed at 500 and 600 °C for a period up to 100h are shown in Figs. 5.15 and 5.16 respectively.

The SEM morphology of corroded surface revealed the oxide layer which formed due to oxidation and hot corrosion (Figs. 5.17-5.26). It may be seen that the salt attack on the surface of the samples non-USSPed and USSPed was very low, from exposure at 400 °C (Figs. 5.17-5.19). However, oxide layer changed with temperature of exposure at 500 and 600 °C (Figs. 5.20-5.26). No oxidised layer was visible in the non-USSPed and USSPed samples, exposed at 500 °C (Fig. 5.27). The thickness of the corroded layer increased with increase in temperature. Rough and thicker oxide layer

was observed on the non-USSPed samples, exposed at 500 and 600 °C, however, dense and continuous oxide layer was observed on the USSPed samples (Figs. 5.28-5.32). The surface became more rough from exposure at 600 °C, compared with that exposed at 500 °C, due to nucleation of oxide particles at the higher temperature [Wen et al. (2012)]. It is obvious that the corroded layer of the USSPed specimen was more dense than the porous oxide layer on the non-USSPed sample.

5.6.1 Effect of 100%NaCl Salt Spray

Type–1 salt sprayed samples showed much higher weight gain (Fig. 5.5, 5.8 and 5.12) as compared to the Type–2 and Type–3 mixed salts sprayed samples. It may be seen from Type–1 salt sprayed samples that oxide scale was cracked due to the presence of NaCl from exposure at 500 and 600 °C (Fig. 5.20 and 5.24). This shows that chloride ions in the atmosphere accelerated the process of cracking of the oxide scale and assisted transmission of oxygen and chloride ions into the material to cause the observed increase in weight gain. Cracks were formed on corroded surface of the alloy because chlorine and oxygen ions could enter easily into the Ti–6Al–4V alloy.

Earlier, Gurrappa (2003) made observation of cracks on the surface of the near α titanium alloy IMI834 and the nickel base alloy CM247LC due to NaCl coating. Logan et al. (1966) proposed cracking mechanism based on diffusion of ions from the oxide scale in particular the chlorine ions from NaCl into titanium alloy and their reaction with alloy constituents to destroy atomic binding forces.

The XRD analysis showed formation of titanium and aluminium oxides. When the alloy Ti–6Al–4V is directly exposed to corrosive environment at elevated temperature, TiO_2 and Al_2O_3 form on the surface of Ti–6Al–4V in oxygen containing

environment, at elevated temperature. Gurrappa (2003) and Anuwar et al. (2007) reported that formation of TiO_2 was the main reaction product followed by that of alumina in titanium alloys at elevated temperatures. Titanium reacts with oxygen to form a non-adherent and non-protective TiO_2 (rutile) which spalls very easily from the base material (Ti–6Al–4V), and aluminium forms protective Al_2O_3 oxide layer. However, this oxide scale of Al_2O_3 started spalling in chloride containing environment at elevated temperature indicating its poor adherence due to presence of chloride ions present in the environment.

As discussed earlier, based on the Gibbs free energy of formation of the different corrosion products at 600 °C, it is obvious that TiO_2 and Al_2O_3 are most feasible products formed due to oxidation reaction. The following reactions are considered to be important in the above process of hot corrosion. Initially an oxide scale consisting of TiO_2 and Al_2O_3 forms on the surface and subsequently these oxide products react with chloride ions from the sprayed salt. The sequence of reactions may be presented as follows:

$$Ti+O_2 = TiO_2 \qquad (5.2)$$

This reaction takes place in air environment in the furnace. TiO_2 is quite protective in nature but reacts with chloride ions present in the saline environment to form volatile $TiCl_4$.

$$TiO_2+4Cl^- = TiCl_4+2O^{2-} \qquad (5.3)$$

$TiCl_4$ is volatile and vaporises at experimental temperature causing cracking in the corrosion products. Further, Al reacts with oxygen present in the furnace to form Al_2O_3.

$$4Al+3O_2 = 2Al_2O_3 \qquad (5.4)$$

Al_2O_3 reacts with chloride ions to form volatile $AlCl_3$

$$Al_2O_3+6Cl^- = 2AlCl_3+3O^{2-} \quad (5.5)$$

$AlCl_3$ becomes volatile in nature at elevated temperatures (the temperature for vaporization of $AlCl_3$ is 178 ºC), hence, causes cracking of the surface. Thus, both the reactions cited above in the equations 5.2 and 5.4 make the oxide scale highly vulnerable for migration of chloride ions and metal cation and enhance the rate of corrosion. This process continues till Ti and Al in the alloy is consumed.

5.6.2 Effect of 75%Na_2SO_4+25%NaCl Mixed Salts Spray

The weight gain was very low in the samples sprayed with Type–2 mixed salts than in those sprayed with Type–1 salt and Type–3 mixed salts. In Type–2 mixed salts, Ti and Al ions react with oxygen ions resulting from decomposition of Na_2SO_4 (Na_2SO_4= Na_2O+SO_3 and SO_3 further decomposes into SO_2 and O_2^-) and forms a non-adherent mixture and non-protective scale of TiO_2; and protective scale of Al_2O_3 respectively. However, NaCl prevented formation of a protective scale in the initial stage, causing internal attack on the two oxides and releasing chlorine as volatile chlorides ($TiCl_4$ and $AlCl_3$). Volatile products formed on the alloy surface. Since, the product $AlCl_3$ is volatile in nature and also surface is nanostructured hence, it is unlikely to develop any network of the said product. TiO_2 and Al_2O_3 also reacted with Na_2O resulting from the decomposition of Na_2SO_4 to form sodium titanate and sodium aluminate as shown below.

$$TiO_2+Na_2O = Na_2TiO_3 \quad (5.6)$$

$$Al_2O_3+Na_2O = 2NaAlO_2 \quad (5.7)$$

The presence of Na_2TiO_3 and $NaAlO_2$ was confirmed by XRD analysis. Gurappa et al. (2003) also reported the above reactions in the presence of 100%Na_2SO_4, 90%Na_2SO_4 +10% NaCl and 90%Na_2SO_4+5%NaCl+5%V_2O_5 on the near α titanium alloy IMI 834.

5.6.3 Effect of 90%Na_2SO_4+5%NaCl+5%V_2O_5 Mixed Salts Spray

In Type–3 mixed salts sprayed sample, corrosion rate was slower than that in the Type–1 salt sprayed sample due to much lower content of NaCl (5wt.%) than those in Type–1 salt and Type–2 mixed salts. In Type–3 mixed salts presence of V_2O_5 led to formation of $NaVO_3$ apart from the oxides TiO_2 and Al_2O_3.

$$Na_2SO_4+2V_2O_5+2NaCl = 4NaVO_3+SO_2+Cl_2 \quad (5.8)$$

The compound $NaVO_3$ is volatile in nature [Sidky et al. (1987)]. The above process continuously progresses till the material degrades. In this study, it was observed that corrosion resistance was improved from ultrasonic shot peening. Tan et al. (2008) observed that corrosion resistance of Incoloy 800H was improved due to conventional shot peening. It is obvious that refinement of grains and much higher density of grain boundaries led to improved corrosion resistance. TiO_2 formation is predominant at elevated temperature (600 °C), however, this oxide is not fully protective and it is easy for oxygen to diffuse inward and dissolve in the substrate. Corrosion products were found to form with development of cavities and pits at grain boundaries, leading to easy flow of oxygen. Initially, at high temperature, a thin outer protective layer is formed on the nano-structured surface which is not fully protective but at the same time an inner protective layer is also formed after breaking of this outer layer (Fig. 5.29).

This inner layer consisted of various oxide products which improved the corrosion resistance of the USSPed samples, thus corrosion resistance of the USSPed samples

was better than those of the non-USSPed samples. Trindade et al. (2005) proposed that the process of oxidation of nanocrystalline material takes place in two parts, one before the formation of protective layer and the other after the formation of protective layer. Before the formation of protective layer, diffusivity of oxygen increases on the shot peened surface, whereas after the formation of protective layer diffusivity of oxygen decreased on the shot peened surface [David (2009)].

The formation of oxide layer was confirmed by WDS analysis. Corrosion resistance depends on effectiveness of the protective layer. It may be seen from the X-ray mapping image, that a nonhomogeneous and adherent scale consisting of mainly aluminium and oxygen was present on the top of the oxide scale (Figs. 5.33 to 5.40). Aluminium and vanadium distribution was smaller and non-homogeneous on the oxide scale, whereas titanium formed a dense oxide and rich layer of titanium oxide (TiO_2 or Ti_2O_3) embedded with small content of aluminium and vanadium above the base material. This layer was more protective in comparison with the other oxide layers. This layer of oxides blocked the penetration of oxygen and other corrosive species to base material. The oxidised layer was distinguishable in cross-section of the corroded samples. Consequentially, corrosion resistance was higher for nanostructured surface as compared to that of the coarse grained non-USSPed Ti–6Al–4V.

5.7 CONCLUSIONS

The following conclusions may be drawn from this chapter:

1) Significant change in weight was observed in the non-USSPed and USSPed samples, exposed at 600 °C, unlike that at 400 °C and 500 °C.

2) Corrosion resistance was enhanced due to surface nanostructure; both of the non-salt sprayed as well as of those sprayed with Type–1 salt (100%NaCl), Type–2 mixed salts (75%Na_2SO_4+25%NaCl) and Type–3 mixed salts (90%Na_2SO_4+5%NaCl+5% V_2O_5).
3) Corrosion resistance was lowest of the sample sprayed with Type–1 salt as compared to those sprayed with Type–2 mixed salts and Type–3 mixed salts.
4) In general, corrosion kinetics was lower in the specimens with nanostructure at surface due to formation of double oxide layer.
5) The main corrosion products were characterised as TiO_2, Al_2O_3, V_2O_3, Ti_2O_3, V_2O_5, and VO_2 in the both, non-shot peened as well as shot peened condition.
6) The oxide layer was changed with temperature and cracking occurred in the oxide layer of the Type–1 salt sprayed specimens from exposure at 500 and 600 °C.
7) The thickness of oxide layer increased with increase in temperature; however the oxide layer was thicker on the non-USSPed sample than that on the USSPed one.